Review and application of stope support design criteria

by A. Daehnke, M. van Zyl, and M.K.C. Roberts*

Synopsis

Stope support systems, typically consisting of props and packs, are used extensively in the gold and platinum mining industry to stabilize the rock mass in the excavation vicinity and to reduce the hazard associated with rockfalls and rockbursts. The design of stope support systems was historically based predominantly on past experience and practices, and cost considerations. The recent development of a new and improved support design methodology, has led to the potential for significant increases in worker safety and support cost savings.

This paper reviews some of the fundamental rock mass and support criteria that form the basis of the improved support design methodology. The considered design criteria are the height of potential fall; quasi-static stope closure rates; dynamic stope closure rates; compressive hangingwall stresses; discontinuity spacing, orientation and interface properties; effect of support length (stoping width); effect of compression rate; consistency of support performance; areal coverage; support spacing; and zone of support influence.

The proposed support design methodology combines both the zone of influence and keyblock stability theories, resulting in optimized support systems for rockfall and rockburst conditions. The site-specific methodology consists of two stages: (i) a tributary area analysis, and (ii) a zone of support influence and a stability analysis, considering hangingwall failure due to buckling, shear and block rotation, which gives maximum safe spacing of individual support units. The methodology is suitable for designing support systems for both blocky hangingwalls and hangingwalls fragmented by face-parallel extension and shear fractures.

Introduction

Stope support systems, typically consisting of combinations of props, packs, tendons and backfill, are used to stabilize the rock mass surrounding stoping excavations and reduce the risk of rockfalls and rockbursts. A paper by Pretorius[1] summarizes both early mining methods and support practice on the central Rand from the early days of outcrop mining. Pillars were the primary in-stope support used and as early as 1895 stamp mill tailings were introduced into some stopes. From the 1920s onwards timber support was used on a large scale as the primary stope support.

Currently, rock related accidents account for in excess of 50 per cent of all fatalities occurring in the mining industry. Of all rock related fatalities, slightly more than half are associated with rockfalls, whilst the remainder are a consequence of the failure of dynamically loaded rock during seismic events and rockbursts. In response to this challenge, a major expansion in research and development effort began in the 1960s. A significant research thrust was, and continues to be, directed at stope and tunnel support, which is recognised as the ultimate strategy to combat the hazards of rockfalls and rockbursts.

The design of support systems has historically been based on experience, past practices and cost considerations. The current methodology generally used by the South African gold and platinum mines to design stope support is based upon the 'tributary area' concept applied to the stope hangingwall. Here, a given weight of rock, determined by an area in the plane of the reef and the height of a possible fall, or the 'fall-out height', is divided between a fixed number of support elements according to the attributable area. The area is determined by the face layout, and the fall-out height is presumed to be known from previous observations. This simple concept takes care of the equilibrium requirements in a rudimentary sense, but it does not adequately address the fact that the rock being supported is likely to be fractured and jointed. Various authors (Klokow[2], Daehnke *et al.*[3]) have found that a high proportion of rock mass instabilities occur *between* support units, and often in the unsupported area between the stope face and permanent support. Clearly, in these circumstances, the distribution of the support elements and the area of hangingwall covered by each unit, are of paramount importance.

At present, it is the responsibility of the

* *CSIR: Division of Mining Technology, P.O. Box 91230, Auckland Park, 2006*

 SA ISSN 0038–223X/3.00 + 0.00. Paper received Jan. 2000; revised paper received Sep. 2000.

rock engineer to estimate support spacing based predominantly upon past experience. In order to improve safety and continue mining at increasing depth, an improved engineering approach is required to design effective support systems with optimum spacing of support units. To this end, an improved understanding of the mechanisms involved in the support–rock interaction, the zones of support influence, maximum stable spans, and the role of rock mass discontinuities is required.

In South African mines, the design of stope support systems has been predominantly empirically based. The lack of a rigorous support design methodology implies that few support systems are optimized, and a considerable amount of over/under-support and/or unsuitable support is used in the permanent support areas of stopes (Roberts[4]). Recent developments (Roberts[4], Daehnke *et al.*[5]) have resulted in improved support design methodologies, which aim to optimize the choice and spacing of support units, while maintaining high levels of safety in rockfall and rockburst conditions.

In the following sections an improved stope support design methodology is proposed. The methodology is based on critical rock mass and support parameters, and takes into account the rock mass condition, zones of support influence, and stable hangingwall spans between adjacent support units. The application of the design methodology will lead to improved hangingwall stability in rockfall and rockburst conditions, and will facilitate optimized support systems in terms of safety and support spacing.

Stope support design methodology

Stope support design has evolved into a comparatively complex discipline involving the quantification of various rock mass and support parameters. Figure 1 gives a flowchart indicating the principal design steps, which should be followed when designing geotechnical area specific support systems. Also indicated in Figure 1, are the relevant sections of this paper, which deal with the specific aspects of support design.

Support design criteria

The improved support design methodology takes into account various critical rock mass and support parameters, which influence the performance and effectiveness of support systems. The following rock mass and support parameters are reviewed in Sections 1 and 2, respectively:

Section 1 Critical rock mass parameters
- *Height of potential fall*
- *Quasi-static stope closure rates*
- *Dynamic stope closure rates*
- *Compressive hangingwall stresses*
- *Discontinuity spacing, orientation and interface properties*

Section 2 Critical support parameters
- *Effect of support length*
- *Effect of compression rate*
- *Support performance variability*
- *Areal coverage of support systems*

Section 3 gives a review of a testing programme to evaluate and quantify the performance of support units under quasi-static and dynamic conditions.

SECTION I

Critical rock mass parameters

Height of potential fall

The most important parameter influencing support design is the height of potential rock mass instability. The fall-out height is used to determine support resistance and energy absorption criteria that a proposed support system would have to meet. The support resistance criterion can be calculated based on the tributary area theory. Here, a given weight of rock, determined by an area in the plane of the reef and the height of possible fall, is divided between a fixed number of support elements according to the attributable area. Thus the support resistance (generally expressed in kN/m^2) is directly proportional to the height of fall, i.e.

$$\frac{F}{A} = \rho\, g\, b \qquad [1]$$

where: F = load carried by support unit (N)
A = tributary area (m^2)
ρ = rock density (taken typically as 2700 kg/m^3)
g = acceleration due to gravity (≈10 m/s^2), and
b = height of fall (m).

Historically, the height of fall has been determined by the rock engineer from *in situ* observations of rock dislodged during rockfalls and rockbursts. Some of these falls occurred in the presence of installed support, while others happened in the unsupported area between the face and permanent support. Discontinuities, such as parting and bedding planes, have a significant influence on the fall height, and, for example in the case of the Carbon Leader Reef, the fall-out height is typically taken as the thickness of the quartzite beam immediately below the Greenbar argillite layer.

Roberts[6] made use of a comprehensive accident database recording all rock-related fatalities on the gold mines since 1990. Cumulative percentage fall-out heights were determined and a criterion set, such that the support system caters for 95 per cent of all rockfalls. The criterion was recently updated (Daehnke *et al.*[5]) to include more recent fatality data. Table I shows the fall-out thickness for the 95 per cent frequency level, i.e. 95 per cent of all falls were the indicated thickness or less. Data are given for (i) rockfall and (ii) rockburst criteria, where, in the rockburst case, the energy absorption criteria are calculated based on an initial hangingwall velocity of 3 m/s. The downward hangingwall movement needs to be arrested within 0.2 m. Further details of energy absorption criteria are given in the subsection dealing with dynamic stope closure rates.

It is emphasized that mines should carry out their own fall-out thickness back-analyses for each Ground Control District (geotechnical area) and should include data from non-casualty causing falls of ground in order to make the analyses statistically relevant. In addition, consideration needs to be given to the position of weak partings in the hangingwall relative to the stope when determining the potential fall-out thickness, as the support, which is installed in the stope, will influence the height to which falls occur.

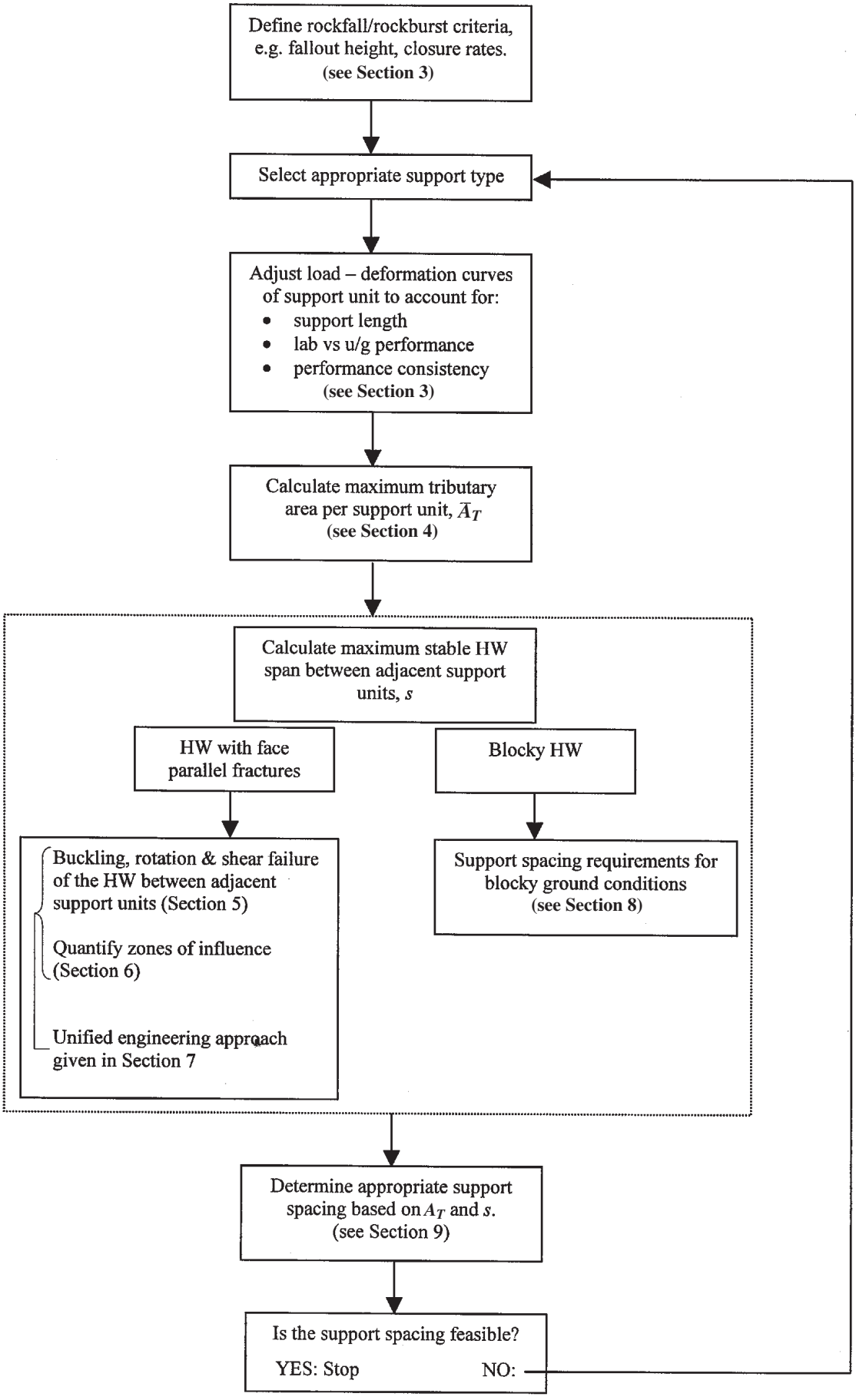

Figure 1—Flowchart indicating principal design steps of support design methodology

Table I

Fall-out thickness for various reefs at 95 per cent frequency level

Reef type	Rockfall		Rockburst	
	Height of fall (m)	Support resistance (kN/m²)	Height of fall (m)	Energy absorption (kN/m²)
Carbon Leader	1.0	27.5	2.2	38.4
VCR	1.2	31.8	1.8	31.4
Vaal	1.2	31.8	1.2	20.9
Basal	1.8	47.7	2.6	45.4

Quasi-static stope closure rates

The quasi-static stope closure rate plays an important role when selecting stope support units for a specific geotechnical environment, as most prop-type support units have a limited yielding range. Generally, if the prop is compressed for a distance exceeding its yielding range, rapid and unpredictable failure due to buckling or punching can occur. Hence, it is important that the yielding range is not exceeded during the prop's required working lifetime. In deep-level mines, where stress-induced fractures are ubiquitous (causing horizontal and vertical dilation), stope closure is significantly higher than the theoretical elastic convergence. The rate of stope closure is dependent on (i) the face advance rate and (ii) time (for example, closure can continue for a period of between 1 and 2 weeks once blasting of the stope face has ceased).

In areas with high closure rates, the prop yield range is expended more rapidly and consequently the energy absorption ability of the support is reduced. Thus, in a high closure, rockburst prone environment, the yield range of props installed close to the face should be at least 400 mm.

It is always preferable that props should be pre-stressed upon installation. In shallow mines the closure rate is generally much lower, and props with a smaller yield potential are adequate. Since the props are loaded at a much slower rate, however, it is especially important to install these props with pre-stressing devices to supply sufficient support resistance and to prevent them from being blasted out when installed suitably close to the stope face. The pre-stressing device should preferably offer an initial load of at least 200 kN, as timber creep can cause a significant drop in the initial pre-stress load.

Dynamic stope closure rates

In seismic and rockburst prone mines, sudden fault rupture or the explosive failure of highly strained rock leads to energy being radiated in the form of stress waves. The stress waves interact with mining excavations, leading to interface and surface waves, energy channelling and wave focusing. The rock is subjected to rapid accelerations, resulting in rock fabric failure, keyblock ejection and stope closure (Daehnke[7], Kirsten and Stacey[8]). The most widely used support design criterion for rockburst prone mines is based on the work of Wagner[9], which takes into account the kinetic and potential energy of the keyblocks. Underground observations, seismic measurements, rockburst back analyses and numerical simulations have indicated that hangingwall blocks can be accelerated to velocities of about 3 m/s. For example, the first generation 1 m/s rapid yield hydraulic props have been observed to occasionally punch into the hanging- and footwall rock during seismic loading, indicating that the props did not yield rapidly enough (i.e. rockburst ejection velocities exceeded 1 m/s). Another example of the occurrence of high peak particle velocities are seismic measurements at Blyvooruitzicht Gold Mine, which indicated a peak velocity of 2.1 m/s over 50 mm (CSIR[10]).

The criterion for effective rockburst resistant support systems is thus to absorb the kinetic and potential energy associated with the hangingwall moving with an initial velocity of 3 m/s. Previously (Roberts[6]), it was assumed that during a rockburst the hangingwall must be brought to rest within 0.2 m of downward movement, i.e. the total energy which had to be absorbed by the support system is:

$$E = \tfrac{1}{2}mv^2 + mgh, \qquad [2]$$

where E is the total energy to be absorbed by the support system, m is the mass of the hangingwall (dependent on fall-out height), v is the initial hangingwall velocity (taken as 3 m/s) and h is the downward hangingwall displacement (taken as 0.2 m).

Hence, the main criterion governing effective support in rockburst conditions is energy absorption, as opposed to support resistance in the rockfall case.

The recommended value of h = 0.2 m is related to the fact that nearly all stopes are at least 0.9 m high. As the movement of underground workers is impaired in stopes less than 0.6 m high, the maximum permissible closure is 0.3 m. Consider an initial quasi-static closure of 0.1 m acting on a prop 5 m from the face (assuming the prop was installed 1 m from the face and that the closure rate is 25 mm/m face advance), the maximum downward movement of the hangingwall during a dynamic event should be limited to 0.2 m. From the preceding discussion, it is evident that the actual value of h is not the same for all stopes, but depends on the initial stoping width, the closure rate and the support resistance and energy absorption capabilities of the support being used. It is therefore recommended that the rock engineer take all of these factors into account when determining the distance over which the hangingwall needs to be arrested.

As is evident from Equation [2], the energy absorption requirements of a support system are linearly related to the downward hangingwall displacement and a function of the square of the peak particle velocity. Thus, a comparatively small increase in peak particle velocity results in a large increase in energy absorption requirements. For example, if the velocity criterion is increased from 3 m/s to 4 m/s, the energy absorption requirement is increased from 6.5 J/kg of rock to 10.0 J/kg (assuming h = 0.2). Thus, an increase in peak particle velocities would set considerably higher energy absorption demands on rockburst resistant support systems.

Compressive hangingwall stresses

Mining-induced fracturing typically occurs at distances of 1 m to 8 m ahead of the stope face for approximate energy release rates (ERR) of 10 MJ/m² to 80 MJ/m², respectively (Jager[11]). The fracturing induces rock dilation, leading to

compressive hangingwall stresses parallel to the profile of the excavation and approximately normal to the stope face and dominant fracture direction (Jager and Roberts[12]).

Compressive hangingwall stresses usually contribute significantly to the rock mass stability (COMRO[13]; Daehnke *et al.*[5]) and tend to stabilize hangingwall blocks that otherwise could rotate or slide out. When attempting to maintain the integrity of a fragmented hangingwall, it is essential to maintain the horizontal clamping stresses. Emphasis should be placed on establishing an even hangingwall surface and maintaining this condition. Hence, from an overall hangingwall stability point of view, it is important to prevent **any** falls of ground, which would leave breaks in the even hangingwall profile. These breaks would disrupt the horizontal clamping stresses, permitting further discontinuity-bounded rockfalls.

Further implications of compressive hangingwall stresses in terms of stable hangingwall spans and zones of support influence are quantified in Sections 5 and 6, respectively.

Discontinuity spacing, orientation and interface properties

It has been shown (Daehnke *et al.*[5]) that the orientation of hangingwall discontinuities has a significant influence on the hangingwall stability and needs to be considered when designing support systems and associated support spacing.

A more densely fractured hangingwall is likely to deform and distort more easily, thus discontinuity spacing needs to be considered during support design. Falls of ground can originate locally, hence increasing the dependence on individual support units, as opposed to an overall effect of the complete support system consisting of multiple props and/or packs. Previous work (Daehnke[14]) has shown that the dependence on individual support units necessitates a more conservative design in order to maintain adequate factors of safety.

In addition, a highly discontinuous hangingwall implies reduced extent of zones of support influence on the immediate hangingwall rock mass (further details and mathematical formulations of zones of support influence are given in Section 6). Thus, for a particular support spacing, the interaction between adjacent support units is diminished and support spacing will have to be reduced in order to maintain stable spans between adjacent units. In order to maintain integrity of highly discontinuous hangingwall beams, increased areal coverage is required (e.g. headboards, nets, link beams, cables, super skins, etc.).

The friction angles of the rock mass discontinuities (bedding surfaces, joints and mining-induced fractures) affect the zone of influence of a support unit. Therefore, interface properties, such as apparent friction angle, need to be considered in the design of support systems (see Sections 5 and 6).

SECTION 2

Critical support parameters

Effect of support length

The force-deformation behaviour of support units can be substantially modified by height. The principal reasons for this are (i) a reduction in stiffness with increasing support unit length, and (ii) an increased potential for buckling.

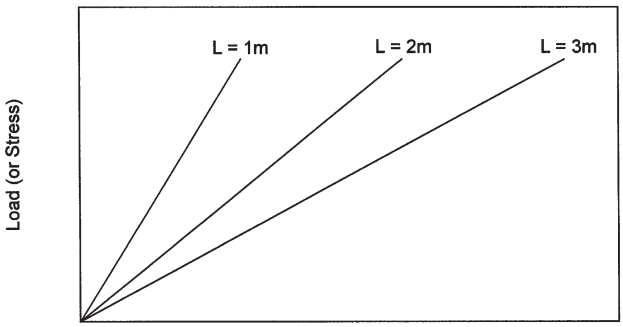

Figure 2—Load versus deformation relationships for various support unit lengths

These factors are discussed in further detail below.

Reduction in stiffness with increasing support unit length

The support resistance generated by a given amount of closure acting on a support unit decreases with increasing length of support unit. Assuming a linear stress-strain relationship during the initial loading phase, i.e.

$$\sigma = E\varepsilon = E\frac{\Delta L}{L} \qquad [3]$$

where: σ = stress transmitted by support unit
E = support stiffness modulus
ε = support strain
L = installed support length (stoping width), and
ΔL = closure acting on support unit.

From Equation [3] it is apparent that, when increasing L (for constant ΔL), the stress transmitted by the support unit is decreased. Thus, for a given stress σ, the deformation ΔL required to generate this stress will double if the length L is doubled (shown graphically in Figure 2).

Increased potential for buckling with increasing support unit length

Generally, with increasing height the support stability decreases, and props and packs in particular are more likely to buckle. The effect of height on the following support units is discussed (Roberts[4]):

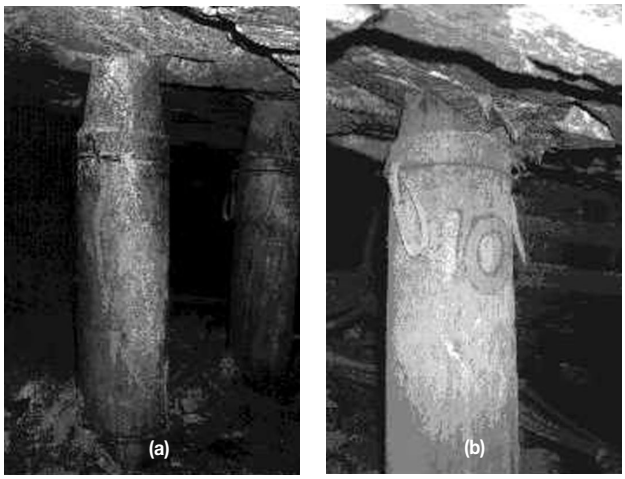

Figure 3—Examples of an installed turned profile prop (note brushing of prop top in *b*)

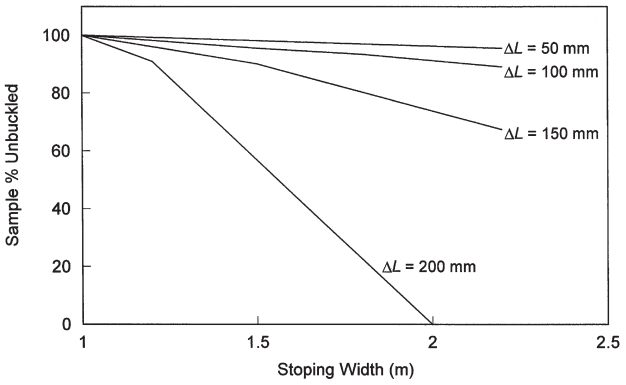

Figure 4—The observed buckling potential of yielding timber elongates (200 mm diameter Profile Prop) as a function of increasing length (stoping width) and stope closure (ΔL)

➤ ***Yielding timber elongates:*** The stability of timber elongates decreases with increasing height and with increasing amount of stope closure. This was determined by means of underground measurements, in which the percentage of buckled 200 mm diameter Profile Props (see Figure 3 for an example of an installed Profile Prop), was determined for various lengths and for various amounts of stope closure. Figure 4 shows this in graphical form, where each curve represents the percentage of buckled props for different amounts of stope closure at various stoping widths (prop lengths).The investigation, from which the data making up Figure 4 is derived, involved measuring hundreds of timber elongates, which had been exposed to various amounts of stope closure. A variety of yielding timber elongate types was included in the survey. Each behaved differently with respect to the buckling potential for different amounts of stope closure. Some had a much higher buckling potential for a given stope closure than the Profile Prop example shown here. With respect to the current generation of yielding timber elongates, no information in this form is available, which is of concern to the authors. Similar investigations, with respect to the underground behaviour of elongate timber support under dynamic loading, have not been undertaken to date.
In order to design support systems for high stoping widths, the force versus deformation curves obtained by means of laboratory compression tests need to be modified to account for the increased buckling potential. The work by Roberts[6] led to the following empirically based buckling adjustment formula for timber elongates (the adjustment formula is based on the underground data presented in Figure 4):

$$\begin{aligned} F &= F_0 && L \le 1.0 \text{ m} \\ F &= F_0\left(1-(L-1)10^{(10\Delta L-2)}\right) && 1.0 \text{ m} < L < 2.5 \text{ m} \\ F &= 0 && L \ge 2.5 \text{ m} \end{aligned} \qquad [4]$$

where: F = adjusted force
F_o = original force determined by means of tests on 1 m elongates
L = length of elongates installed underground, and
ΔL = displacement (compression).

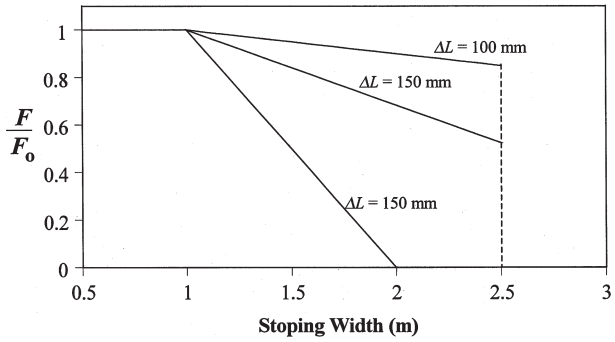

Figure 5—Buckling adjustment for elongate systems versus stoping width (based on empirical data of 200 mm diameter Profile Props by Roberts[6])

Figure 5 graphically depicts the buckling adjustment of timber elongate systems for various values of displacement ΔL. As is apparent from Figure 5, regardless of the displacement ΔL, timber elongates are assumed to fail in the buckling mode at lengths in excess of 2.5 m. Whilst this might be an over-conservative assumption for rockfall conditions, it is applicable in rockburst conditions, where timber elongates are particularly prone to buckling during rapid stope closure.
To gain further insights into the effect of high stoping widths on the buckling potential of elongates, an approach based on column analysis is adopted. Elongates can be considered as columns, where the stress may be considered partly due to compression and partly due to bending. Hence, two column theories are used, namely (i) the Euler column theory for *long columns*, and (ii) the Johnson column theory for *short columns* (Shigley[15]). The expressions for the critical load at the onset of buckling for the two column theories are given below.

$$\text{Euler column}: \quad \sigma_{cr} = \frac{E\pi^2}{(L/k)^2} \qquad [5]$$

$$\text{Johnson column}: \quad \sigma_{cr} = a - b\left(\frac{L}{k}\right)^2 \qquad [6]$$

where: σ_{cr} = critical column stress at the onset of buckling (Pa)
k = radius of gyration = $d/4$ for a solid circular column of diameter d (m)
L = column length/stoping width (m)
E = Young's Modulus (P), and
a, b = constants.

The constants a and b are adjusted to cause the Johnson column formula to fit experimental data. One of the most widely used versions of the Johnson column formula entails setting the constants as follows (Shigley[15]):

$$a = S_y \qquad [7]$$

$$b = \frac{1}{E}\left(\frac{S_y}{2\pi}\right)^2 \qquad [8]$$

where S_y is the yield strength of the material.

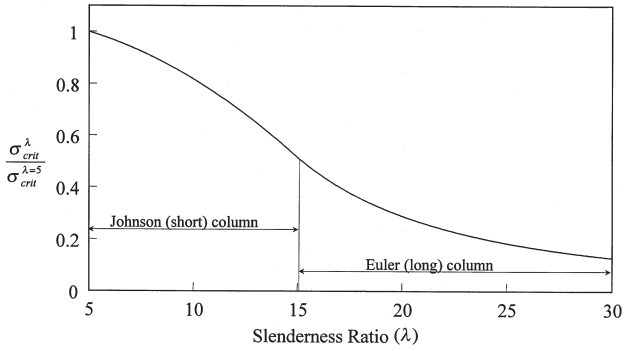

Figure 6—Normalized σ_{crit} versus slenderness ratio based on the Johnson and Euler column buckling theories

Extensive laboratory compression tests on minepoles (Daehnke *et al.*[16]) indicate an average Young's Modulus of E = 4.0 GPa (taken as the average slope of the approximately linear force-deformation curve during the initial loading phase). The average yield strength of the minepoles was found to be S_y = 22.7 MPa. The Young's Modulus and yield strength are downgraded from a laboratory compression rate of 1 mm/min to typical underground closure rates of 10 mm/day, giving adjusted values of E = 3.3 GPa and S_y = 18.6 MPa (see the following section for further details on the effects of loading rate).

Figure 6 gives values of σ_{crit} (normalized with respect to σ_{crit} at a slenderness ratio of 5). The slenderness ratio is defined as $\lambda = L/d$, where L and d are the length and diameter of the prop, respectively.

The use of Figure 6 is illustrated by means of an example: Compression tests on a minepole (L = 1.0 m, d = 0.15 m and $\therefore\lambda$ = 6.7) indicated a peak load capacity of 260 kN (i.e. σ_{crit} = 14.7 MPa) before the onset of buckling failure. To estimate the peak load capacity of a minepole with L = 2.0 m, d = 0.15 m ($\therefore\lambda$ = 13.3), the ratio of normalized values of $\sigma_{crit}^{\lambda=13.3}$ = 0.63 and $\sigma_{crit}^{\lambda=6.7}$ = 0.95 (determined from Figure 6) is used to downgrade the load capacity. Thus $\sigma_{crit}^{\lambda=13.3} \div \sigma_{crit}^{\lambda=6.7}$ =0.66 times the peak load capacity of the 1 m long minepole (260 kN, 14.7 MPa) gives a load capacity of 172 kN (9.7 MPa) for the 2 m long minepole before the onset of buckling.

The column theories applied here are applicable for estimating the increased buckling potential as the length of minepoles is increased. In the case of the new generation yielding elongates, the adjustment of load capacity for increased elongate length is complicated by the yielding mechanism of the prop. At this stage, no general formulae to adjust for increased buckling potential (applicable to all yielding elongate types) have been developed. It is necessary that *in situ* and laboratory force-deformation data of elongates tested at the appropriate length be used to quantify actual elongate performance. If the elongate performance data for the required stoping width is not available, further tests need to be conducted, making use of elongates of the corresponding length.

- **Timber packs:** It is known that the stability of packs also decreases with increasing height. For example, it is commonly assumed that timber packs with height-to-width ratio exceeding 2:1 are unstable, particularly during dynamic closure. This is a qualitative assessment from underground experience. However, the pack type has an influence on the buckling potential with the stiff end-grained packs having a higher buckling potential than conventional mat packs. An example of a composite timber/brick pack is given in Figure 7.

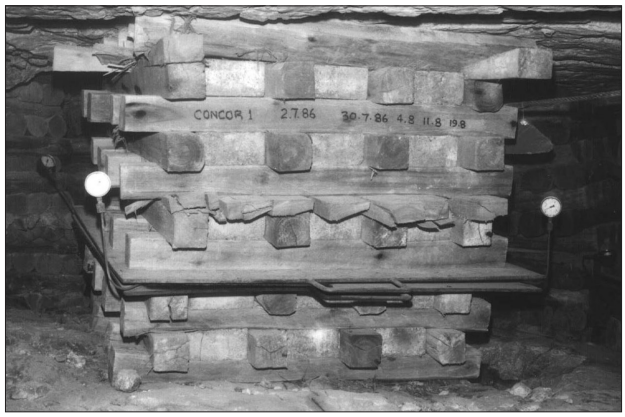

Figure 7—Example of a composite timber/brick pack. Note the instrumented flatjacks used to record the pack load

- ***Hydraulic props:*** The stability of hydraulic props (Figure 8) has been greatly improved in recent years by the adoption of conical extension pieces. The blast-out rate of hydraulic props increases with increasing prop length. A number of years ago, 8 t blast-on props were used at a number of mines. They are not currently used, but blast-out data was determined and is presented here. It was shown that for these lightweight 8 t blast-on props, the blast-out rate for the front line of props increases significantly for stoping widths above 1.5 m. Hence, it was recommended that 80 kN hydraulic props should not operate in stoping areas where the stoping width exceeds 1.5 m and, furthermore, the front row should not be closer than 1.2 m from the stope face. With respect to 20/40 t rockburst hydraulic props, now the standard hydraulic prop, the blast-out rate with increasing stoping width has not been determined in a systematic manner underground. However, underground observations

Figure 8—Example of a stope with 20/40 t rockburst hydraulic props installed 1 m from the stope face

have indicated that, if these types of hydraulic props and extensions exceed 2.0 m in length, they may become unstable during dynamic loading. The mass of such props makes them difficult to handle and install, particularly in stopes, where dip angles exceed 25°.

- ***Mechanical props:*** Testing of mechanical props with respect to their stability with increasing length was undertaken by Roberts[6]. A variety of mechanical props were tested, primarily to determine the buckling potential with increasing length and, secondly, to determine their ability to absorb energy. It was found that between the lengths of 2.3 m and 2.7 m, the props failed by buckling at loads below 120 kN and at progressively lower loads with increasing lengths.

Effect of compression rate

Various studies (Roberts *et al.*[17]; Daehnke *et al.*[5]) have been conducted to quantify the force-deformation characteristics of elongates installed in working stopes underground. It was shown that the force-deformation behaviour of the support units can be significantly downgraded compared to the laboratory derived force-deformation curves. To clarify this discrepancy, a series of systematic laboratory tests (Roberts *et al.*[17]) was carried out to assess the influence of various parameters, including temperature, humidity, timber quality and loading rate, on the performance of timber props. It was found that the differences in loading rate (10–30 mm per minute during laboratory tests versus 5–30 mm per day underground) had the greatest effect on reducing the support load when comparing laboratory and underground test results.

The materials constituting a particular support type or the yielding mechanisms can render the support performance loading-rate dependent. For example, the strength of timber is generally known to be rate dependent and at higher loading rates the strength of a timber based support element increases. This implies that support units, such as timber elongates and packs, offer higher support resistance when tested in the laboratory compared to their underground performance. Conversely, during rapid stope convergence, such as typically encountered during rockbursts and dynamic events, the support resistance of packs and timber props is increased significantly.

Props making use of frictional yielding mechanisms result in lower support resistance during rapid compression. This is due to the fact that the coefficient of dynamic friction is generally lower than the coefficient of static friction.

Correction factors have been derived, which allow rock engineers to assess the likely underground performance of a particular support unit from laboratory derived force-deformation curves. The following equations adjust the support resistance of timber elongates and packs for loading rate (Roberts[6]; Lightfoot[18]; Pretorius[19]):

$$\text{Timber elongates:} \quad F_{u/g} = F_{lab}\left[m \log\left(\frac{v_{u/g}}{v_{lab}}\right) + 1\right] \qquad [9]$$

$$\text{Timber packs:} \quad F_{u/g} = F_{lab}\left(1 + \frac{16}{100}\right)^{\log\frac{v_{u/g}}{v_{lab}}} \qquad [10]$$

$$\text{Cementitious packs:} \quad F_{u/g} = F_{lab}\left(1 + \frac{10}{100}\right)^{\log\frac{v_{u/g}}{v_{lab}}} \qquad [11]$$

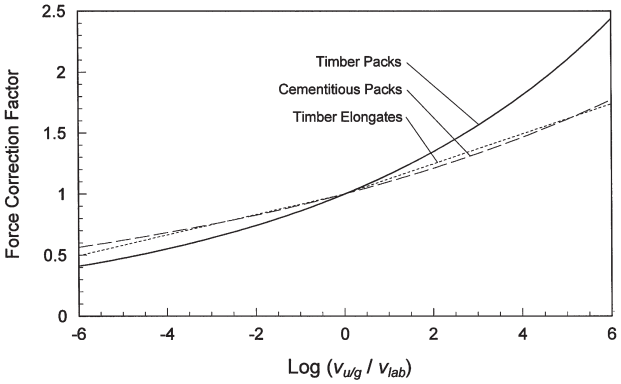

Figure 9—Graphs used for adjusting the load-deformation curves for different deformation rates

where: $F_{u/g}$ = adjusted force
F_{lab} = original force as measured during laboratory test
$v_{u/g}$ = underground site velocity (typically 1 – 3 m/s for rockbursts and 1–30 mm/day for rockfalls)
v_{lab} = laboratory compressive rate (typically 10–30 mm/min)
m = empirically determined correction factors,
where: m = 0.123 for rockbursts, and
m = 0.084 for rockfalls.

The above equations can be rewritten as $F_{u/g} = k\,F_{lab}$, where k is the force correction factor. A graphical representation of the force correction factors for different velocities can be found in Figure 9 for timber elongates and for timber and cementitious packs.

For example, if v_{lab} = 30 mm/min and $v_{u/g}$ = 10 mm/day = 0.007 mm/min, then $\log\left(\frac{V_{u/g}}{V_{lab}}\right)$ =–3,6. From Figure 9 it can be seen that this gives a force correction factor for timber elongates of 0.69. Thus, $F_{u/g} = 0.69F_{lab}$.

Support performance variability

To evaluate the effect of the inherent strength variability associated with elongates, a statistical method is presented by Daehnke[14], which addresses and quantifies the consistency of support performance. The analysis, which is based on a normal distribution, makes use of force-deformation curves determined from multiple laboratory compression tests on the same support type. The applicability of the method is illustrated making use of actual performance capabilities of various types of elongates.

In order to ensure a high probability that support units installed underground exceed the standard support performance curve (established by means of laboratory tests), the statistical mean of a suite of tests, based on the same support type is downgraded. The 'correction factor' ($\bar{x}$) is a function of the mean (μ) and standard deviation (σ) of the test data, as well as the sample size (n) of units deemed necessary to control the local rock mass stability. It is shown that downgraded performance curves, based on a high probability of 90 per cent (if n = 1: $\bar{x} = \mu - 1.282\sigma$) or 95 per cent (if n = 1: $\bar{x} = \mu - 1.645\sigma$) of support units exceeding this performance level, are suitable to ensure that the design

Table II

Relating $\bar{x}$, μ and σ for probability levels of 90, 95 and 99 per cent, and n = 1, 3, 10 and 30

Probability of exceeding performance specification			
	90 %	**95 %**	**99 %**
$n = 1$	$\bar{x} = \mu - 1.282\sigma$	$\bar{x} = \mu - 1.645\sigma$	$\bar{x} = \mu - 2.326\sigma$
$n = 3$	$\bar{x} = \mu - 0.740\sigma$	$\bar{x} = \mu - 0.950\sigma$	$\bar{x} = \mu - 1.343\sigma$
$n = 10$	$\bar{x} = \mu - 0.405\sigma$	$\bar{x} = \mu - 0.520\sigma$	$\bar{x} = \mu - 0.736\sigma$
$n = 30$	$\bar{x} = \mu - 0.234\sigma$	$\bar{x} = \mu - 0.300\sigma$	$\bar{x} = \mu - 0.425\sigma$

of support systems will invariably meet the design criteria in practice (Table II). This specification aims towards high levels of safety, whilst rationalizing the support costs and practical difficulties associated with installing high-density support systems.

In the highly discontinuous hangingwall rock mass typically associated with intermediate- and deep-level mining operations, the interaction between adjacent support units is comparatively limited, as seen by the more common fall-out between support units, rather than failure of the units themselves. Therefore, the appropriate sample size (n) of the support units controlling the *local* rock mass stability should be $n = 1$. In shallow mining conditions, sample sizes of up to $n = 10$ may be warranted, depending on the spacing of joints and other discontinuities in the hangingwall.

To advance the design of support systems and continue mining at ever-increasing depths with reduced rock-related risk, design methodologies need to be based upon sound engineering principles. A probabilistic approach is particularly suited to assessing, quantitatively, rock mass behaviour and support performance. Although many aspects of the interaction of support with the hanging- and footwall rock mass are poorly defined and understood, it is nevertheless necessary to quantify comparatively straightforward design parameters, such as the inherent variability of support systems.

Areal coverage of support systems

The predominant reason leading to falls of ground in stopes is inadequate areal coverage. The majority of FOGs occur between support units and generally support units fail purely mechanically only under severe dynamic loading (Jager and Ryder[20]). Maximizing areal coverage is thus critical to reduce FOG casualties.

A basic measure of the areal coverage of a support system is the percentage that the contact area of the support units makes of the total area of hangingwall to be supported. For typical prop and elongate systems this figure is less than 1 per cent and for pack systems generally less than 10 per cent.

Areal coverage is typically increased by installing props with headboards. Recent developments by CSIR Division of Mining Technology have resulted in alternative support systems offering extensive areal coverage. Examples of these are shown in Figure 10.

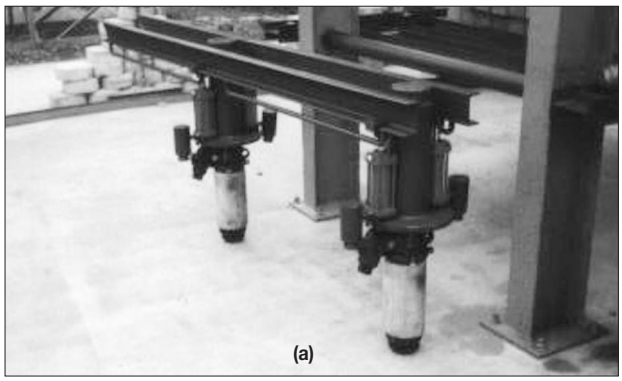

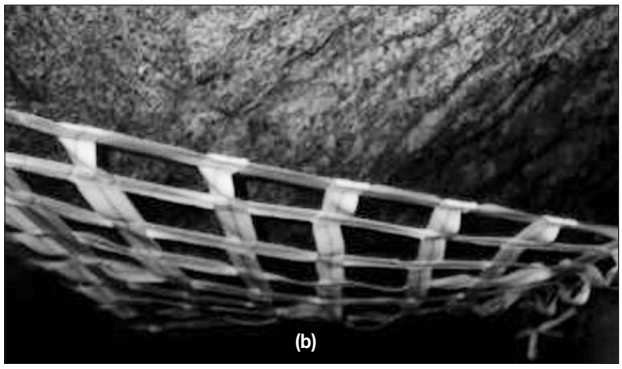

Figure 10—(a) Twin beam support system providing good areal coverage in the strike direction (after Kuijpers[21]).
(b) Nets spanned between props provide extensive areal coverage and reduce the rock-related hazard between support units.
(c) Spray on membrane, here applied to a tunnel sidewall, can be applied to the stope hangingwall to offer 100% coverage in the applied area.

SECTION 3

Testing programme to evaluate support performance

As part of the work conducted by Daehnke *et al.*[5], a provisional test procedure has been proposed to provide a systematic approach to the performance evaluation of elongates. The test procedure entails various laboratory and underground compression tests of the support units, with

emphasis placed on repeated tests using units of the same type to investigate performance variability and obtain a statistical distribution of the load versus deformation curves.

The complete testing programme requires 27 support units of the same type. The testing programme includes 5 rapid displacement and 2 creep tests. Support units that are not designed for seismically active mines are not subjected to rapid displacement testing. For mines with convergence in excess of 2 mm/day, no creep tests are necessary. The full suite of tests entails determining the force versus deformation curves of the following laboratory and underground compression tests:

- Ten slow tests at a loading rate of 30 mm per minute. The units are tested to destruction or to a yield level specified by the manufacturer (maximum: 500 mm).
- Five rapid displacement tests at 3 m per second for 200 mm. The loading rate should be 30 mm per minute prior to and subsequent to the rapid displacement. Initial displacement to be 50–100 mm before initiation of the rapid displacement. The units are tested to destruction or to a yield level specified by the manufacturer (maximum: 500 mm).
- Three slow tests at a loading rate of 30 mm per minute on a 10 degree grooved platen. The units are tested to destruction or to a yield level specified by the manufacturer (maximum: 500 mm).
- Two creep tests. Units with pre-stressing devices will be set at 200 kN. Units with no pre-stressing devices will be set at 80 kN. The units will be loaded by the initial compression and their load shedding monitored for a period of seven days. The creep tests can be terminated earlier provided that no load shedding occurs.
- Two slow tests at a loading rate of 10 mm per day for a period of seven days.
- Five underground force-deformation tests using load cells and a suitable closure measuring device.

While it is recognised that this number of tests is comparatively small, particularly to facilitate an accurate statistical data analysis and interpretation, the number of tests is nevertheless deemed adequate to give important insights into the performance variability associated with various elongate types, and to establish elongate design curves suitable for use in the mining environment. Support manufacturers should conduct routine quality testing of their products, and these data should be accumulated to augment the original statistical results.

The elongate support unit performance specification is determined as follows:

- Calculate separately the means of the ten standard- (30 mm/min compression rate), the five rapid displacement- (3 m/s compression rate), and the five underground compression tests. Assuming a normal distribution, calculate the support performance curves that ensure a probability of 90 per cent (mean – 1.282 standard deviation) and 95 per cent (mean – 1.645 standard deviation) of exceeding the support capability. The performance curves are calculated for the ten standard, the five rapid, and the five underground compression tests. The choice of either the 90 per cent or 95 per cent performance curve rests with the rock engineer for his/her particular application and safety margin.
- The 90 per cent or 95 per cent performance curves should be related to the underground tests, and downgraded further if necessary. By establishing a relationship between the laboratory and underground test results, further quality assurance testing can be limited to laboratory tests. The underground support performance can then be inferred from the laboratory test results.
- Finally, the adjusted laboratory test curve, which has been further downgraded to the underground test results, represents the elongate support unit specification that should be used in support design.

The final adjusted curves for the various support types should then be used to select support for specific geotechnical environments. This will depend upon factors such as (i) energy absorption and support resistance requirements, (ii) initial stiffness requirements, (iii) yielding capabilities, and (iv) closure rates in the particular environment.

It is recommended that the appropriate performance curves be used when designing support systems for seismic and non-seismic applications. In some cases, the support bearing capacity of elongates increases during dynamic loading (e.g. timber elongates), whilst in others the loading capacity decreases (friction props, e.g. Rocprop). Thus, a single correction factor for various elongate types loaded under quasi-static and dynamic loading conditions is not applicable, and separate performance curves, based on laboratory and *in situ* tests, are required.

SECTION 4

Stope support design based on tributary area theory

The tributary area theory is the basis of support design. Irrespective of the extent of zones of influence and stable spans between adjacent support units, the tributary area criteria should be met at all times. The tributary area requirements for rockfall and rockburst conditions are reviewed below.

Tributary area requirements for rockfall conditions

Figure 11 gives the maximum tributary area (A_T) that can be supported by a single support unit for rockfall conditions. The tributary area is given as a function of the height of potential rock mass instability and support force. The height of instability (b) is commonly governed by the position of bedding surfaces, and should be determined from previous rock mass instabilities and falls of ground.

The basic tributary area relationship, $F = \rho\, g\, b\, A_T$, can be re-written as:

$$A_T = \frac{F}{\rho\, g\, b}, \qquad [12]$$

where: A_T = maximum potential tributary area (m^2)
F = support unit load (N)
ρ = rock density (2700 kg/m^3)
g = acceleration due to gravity (10 m/s^2), and
b = height of instability (m).

Figure 11 shows the relationship given by Equation [12] graphically.

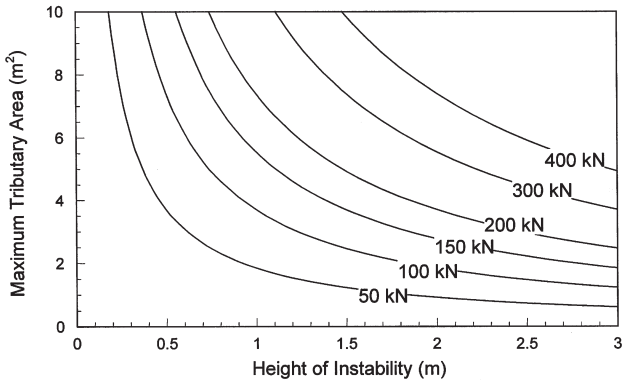

Figure 11—Tributary area requirements for rockfall conditions

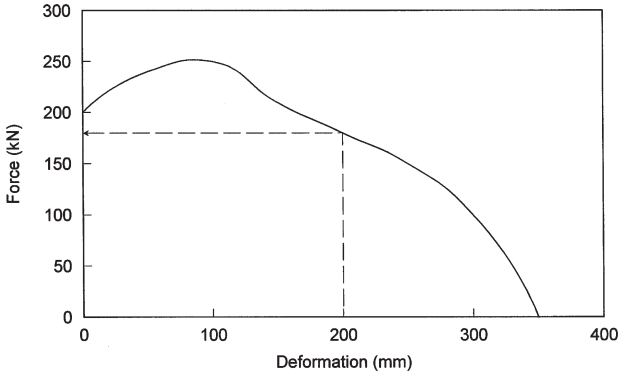

Figure 12—Design force versus deformation curve of hypothetical support unit (in this example the support unit was initially pre-stressed to 200 kN)

Assume that a support unit with the force versus deformation characteristics shown in Figure 12 is used. It is further assumed that the closure rate, as measured in the stope, is 20 mm per metre of face advance, and the support unit should maintain rock mass stability as the face is advanced a further 10 m. This implies that for at least 200 mm of closure the support unit needs to carry sufficient load to meet the tributary area requirements.

At 200 mm deformation the support unit carries a load of 180 kN. For the rock mass to be stable over this deformation range (based on the tributary area criterion), the maximum tributary area should not exceed 4.5 m^2 (determined from Figure 11, assuming F = 180 kN and b = 1.5 m).

The distance from the stope face, at which the support system needs to be installed to ensure rock mass stability (i.e. in the above example: 10 m + support installation distance from the face), is an important support design consideration. This distance should at least extend to the sweeping line (typically 5–6 m from the face), and preferably into the back-area, of the stope (Figure 13). By ensuring the support performance criteria are met for this distance, the rock mass stability is maintained over an area extending at least up to the sweeping line.

Tributary area requirements for rockburst conditions

Energy absorption (rockburst) requirements based on the tributary area criterion follow analogously to the support resistance (rockfall) case. Figure 14 gives the maximum tributary area as a function of the height of instability and the energy absorption capacity of the support unit. The relationship is based on the well-known kinetic and potential energy absorption criterion (Wagner[9]), i.e.

$E_a = 0.5\ m\ v^2 + m\ g\ h$, where $m = \rho\ b\ A_T$.

The relationship is re-written as:

$$A_T = \frac{E_a}{\rho\ b\left(0.5v^2 + gh\right)}, \qquad [13]$$

where: A_T = maximum potential tributary area (m^2),
E_a = energy absorption capacity of the support unit (J),
ρ = rock mass density (2700 kg/m^3),
b = height of instability (m),
v = rock ejection velocity (3 m/s),
g = acceleration due to gravity (10 m/s^2), and
h = hangingwall displacement during dynamic event (0.2 m).

The use of Figure 14 is illustrated by means of an example. Assume that a support unit is used with a force

Figure 13—Stope plan view indicating minimum distance behind face over which the support performance criteria must be met

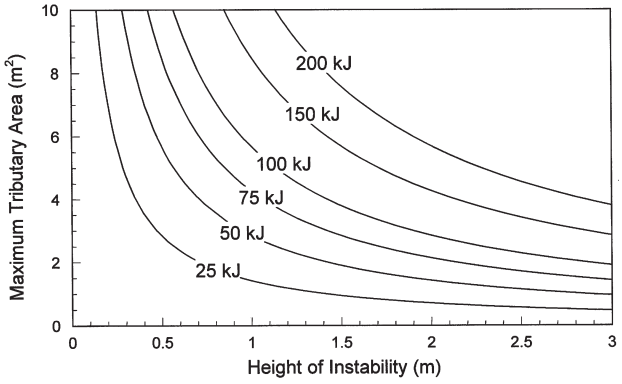

Figure 14—Tributary area requirements for rockburst conditions

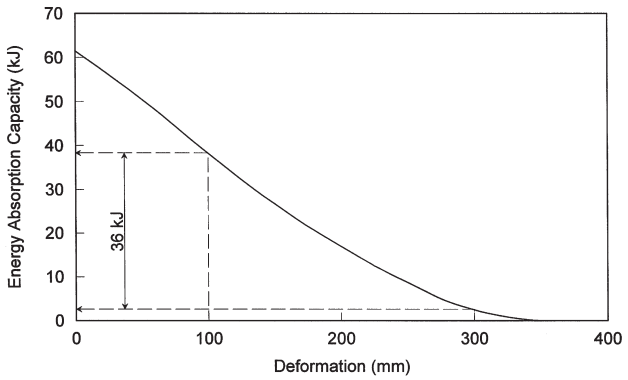

Figure 15—Remaining energy absorption capacity of the hypothetical support unit

versus deformation curve, as shown in Figure 12. The design requirements are that, as the face is advanced a further 5 m, the support unit must maintain rock mass stability during a rockburst and retain a support resistance after dynamic deformation of *mg*. Stope closure is 20 mm per metre of face advance, i.e. the support unit needs to maintain rockburst stability after having been compressed by up to 100 mm of quasi-static closure. Figure 15 graphically illustrates the remaining energy absorption capacity of the support unit (calculated by the area under the force versus deformation curve).

From Figure 15 it is apparent that after 100 mm of deformation, 38 kJ of energy absorption capacity remains available. The hangingwall is assumed to displace dynamically over a distance of 0.2 m, i.e. up to 300 mm total deformation. At this point only 2 kJ energy absorption capacity remains. The change in energy absorption capacity, i.e. $\Delta E_a = E_a(100\ \text{mm}) - E_a(300\ \text{mm}) = 36$ kJ, is the amount of energy available. The tributary area criterion is based on this amount of energy, i.e. in this example 36 kJ. From Figure 14 it is apparent that the maximum tributary area should not exceed 1.5 m^2 (assuming $E_a = 36$ kJ and $b = 1.5$ m).

Two further criteria, which need to be considered when designing rockburst resistant support systems, are:

- The load carried by the support unit after the rockburst must exceed the corresponding tributary area load. In this example $F(300\ \text{mm}) = 100$ kN, which is adequate to support the tributary area load = $\rho\ g\ b\ T_A = 61$ kN. (If the load carried by the support unit after the rockburst is less than the tributary area load, a different support unit should be chosen or the support spacing reduced.)
- The stoping width minus the total closure after the rockburst should be adequate to prevent injury to, and allow movement of, mine personnel. A minimum post-rockburst stoping width of 0.6 m is recommended, i.e. in the example given here the initial stoping width should not be less than 0.9 m.

In the design method given here, a dynamic hangingwall displacement of 0.2 m is assumed. In practice the downward movement of the hangingwall is dependent on the support reaction and, for example, a support system providing high support resistance will arrest the hangingwall within a shorter distance. In this case, the potential energy component is decreased and hence the total energy absorption requirements are reduced. In practice, most support systems will decelerate the hangingwall over a distance less than 0.2 m. The $h = 0.2$ m assumption made here is conservative. To fully optimize support systems, the use of the SDA II software is recommended, where the value of h is explicitly calculated for each support unit.

Tributary area requirements related to stope closure

Roberts[4,6] proposed a design methodology based on tributary area theory comparing the actual support resistance and energy absorption of the system with the respective criteria at any distance from the stope face, taking into account the effects of stope closure.

Any support units installed in a stope are immediately acted upon by stope closure. Depending on the force-deformation characteristics of the support unit, this closure could either degrade or increase its ability to generate load. In order to take this into account, it is necessary to represent a support system as a support resistance-deformation curve, which is a function of stope closure and thus of the distance behind the stope face. The support resistance-deformation curve is determined from the load-deformation curve of the support unit by dividing the load-bearing capacity of the support unit by the tributary area associated with the support unit.

Figure 16 is a graphical representation of the design method. The upper section is the support resistance–deformation graph for the proposed system being evaluated. The lower section is a nomogram that converts distance behind face to compression of the support units for various rates of closure expressed in mm/m (mm of closure per metre of face advance); or equivalently, if the face advance rate is specified, in terms of mm/day. The method also takes into account the distance behind the face that the support is installed by starting the closure rate lines on the y-axis at this distance.

The graphs can be used to determine the support resistance for any distance behind the stope face and for any closure rate. In the example, the support is assumed to have been initially installed 3 m from the stope face and the stoping is on a 2-day cycle. Considering point **A** some distance behind the stope face, a horizontal line is traced until it intersects the line representing the stope's closure rate at point **B**. From **B** a vertical line is traced to intersect the

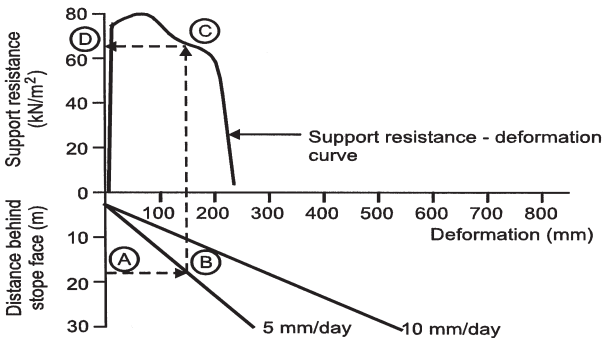

Figure 16—A support resistance–deformation design chart for rockfall conditions, which allows stope closure and distance behind the stope face to be taken into account

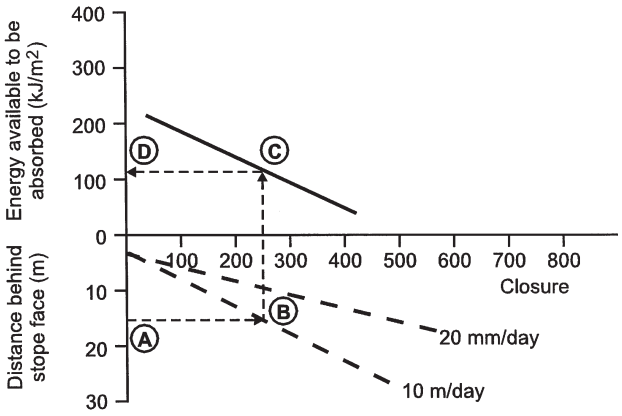

Figure 17—An energy capacity—deformation design chart for rockburst conditions, which allows stope closure and distance behind the stope face to be taken into account

support resistance-deformation curve of the support system at point **C**. From **C** a horizontal line is traced back to the y-axis at **D**, where the support resistance of the support system at that particular distance from the face for the specific closure rate can be read off.

In the case of support design for rockburst conditions, energy capacity curves, as opposed to support resistance curves, are used. A process similar to that introduced for the rockfall design can be followed, except that now the support performance is tested against the hangingwall energy criterion (defined in Section 3).

Figure 17 combines the graph of energy capacity with a nomogram in the lower half of the diagram, which relates the amount of stope closure experienced by a support unit installed a specific distance behind the stope face for various rates of closure. Consider some distance behind the stope face, point **A**. A horizontal line is traced from **A** until it intersects the line representing the stope closure rate, point **B**. From **B** a vertical line is traced to intersect the energy-deformation curve of the support system, point **C**. From **C** a horizontal line is traced back to the y-axis at **D**, where the available energy can be read off and compared to the energy criterion.

Further details of the support design methodology outlined above are given by Roberts[4] and Jager and Ryder[20], where an approach to separating the face and permanent support areas, as well as combining multiple support types, is given.

SECTION 5

Quantifying stable hangingwall spans between support units

This section reviews a formulation (Daehnke *et al.*[22]) for quantifying stable hangingwall spans between support units and assessing the influence of rock discontinuities on stable hangingwall spans. Hangingwall span stability is assessed by considering two failure mechanisms, namely (i) beam buckling, and (ii) shear/rotational failure due to slip at the abutments.

Hangingwall beam buckling

The design procedure to quantify the stability of a Voussoir

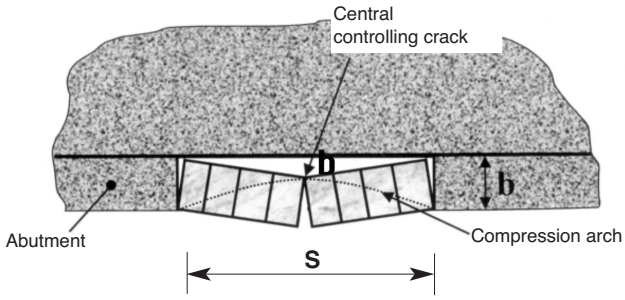

Figure 18—Voussoir beam geometry for hangingwall beam analysis

beam is based on that developed by Evans[23], and subsequently modified and extended by Beer and Meek[24], Brady and Brown[25], and Hutchinson and Diederichs[26]. The solution technique follows the intuitive idea that, in a discontinuous hangingwall beam, the central transverse crack determines the deformational behaviour (Figure 18). In the buckling mode the beam becomes unstable to form a 'snap-through' mechanism.

The relationship between stable span and beam thickness is highly dependent on the *in situ* rock mass stiffness measured in a direction parallel to the excavation surface. The *in situ* rock mass stiffness is predominantly governed by the stiffness of the rock mass discontinuities, and is lower than the stiffness of solid rock, which is characterized by the Young's modulus.

Bandis *et al.*[27,28] made use of experimental data to establish a relationship between normal joint stiffness and normal stress for well-interlocked joints in various rock types. These data are used to establish a relationship between stable span and beam thickness. Multiple discontinuities act as springs in series, and it is assumed that each discontinuity is compressed equally. Span versus thickness relations, shown in Figure 19, give the stability envelopes of hangingwall beams with 3 joints, as well as 1, 3, 5, 10 and 100 joints per metre of hangingwall length. Daehnke *et al.*[22] give further details of the assumptions made when calculating maximum stable spans of hangingwall beams failing in the buckling mode.

Shear and rotational failure by slip at the abutments

The second failure mechanism considered by Daehnke *et al.*[22]

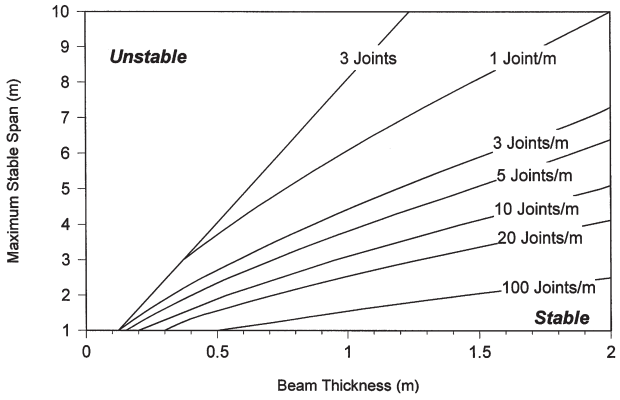

Figure 19—Buckling stability envelopes of a discontinuous hangingwall beam

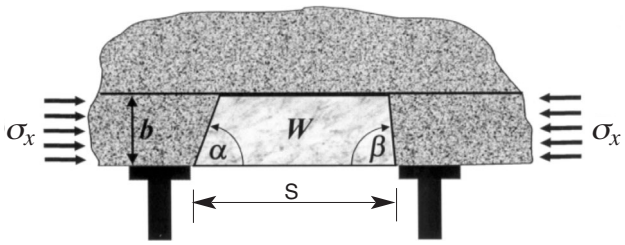

Figure 20—Potential keyblock instability due to shear failure at the abutments

is shear and rotational failure by slip at the abutments. Figure 20 is a schematic diagram of the geometry governing the stability of a hangingwall keyblock. The weight of the block is denoted by W, the beam thickness by b, the span between adjacent support units by s, and σ_x is the magnitude of compressive horizontal stress in the hangingwall. Finally, α and β are the angles that define the orientation of the extension and shear fractures, respectively. The stability of the largest possible keyblock is investigated, i.e. the block geometry is defined by extension and shear fractures terminating at the hangingwall surface immediately next to the support units. It is assumed that all partings have no cohesion. This is a realistic assumption as shearing parallel to the bedding is common in intermediate and deep mines, destroying any inherent cohesion. The horizontal hangingwall stress, acting perpendicular to the stope face, is generated by two mechanisms, namely rock dilation and block rotation (Daehnke *et al.*[22]).

The discontinuities, which represent mining-induced fractures, are assumed to have zero cohesion on the inclined contact (fracture) surfaces. Hence, for the keyblock to be stable, the lateral thrust at the abutments, due to *in situ* compressive hangingwall stresses, must mobilize a frictional resistance sufficient to balance the abutment shear force.

Stability or instability of the keyblock depends on various factors. The criteria for stability are summarized as follows:

- *Unconditional stability.* The keyblock is unconditionally stable (Figure 21a) if the forces and moments are both in equilibrium. The forces will not induce the fall of the block if $V_I + V_{II} > W$. Similarly, the moments will not cause dislodging movements (rotation) if the supporting forces satisfy the following inequalities: $V_I > {}^1/_2 W$ and $V_{II} > {}^1/_2 W$. Obviously, if the two conditions concerning moments are satisfied, the first criterion will also be fulfilled. The conditions for unconditional stability can be expressed as follows (Daehnke *et al.*[22]):

$$\alpha > \frac{1}{2}\pi \pm \phi \text{ and } \beta > \frac{1}{2}\pi \pm \phi. \quad [14]$$

- *Conditional stability.* If only the criterion concerning forces and *one* of those arising from moments are satisfied, then the block may or may not be stable. To illustrate such a situation, postulate the following:

$$V_I + V_{II} > W; \quad V_I < \frac{1}{2}W; \quad V_{II} > \frac{1}{2}W. \quad [15]$$

Clearly this block is not unconditionally stable, but it may *not* get dislodged if its rotation is *kinematically impossible.*

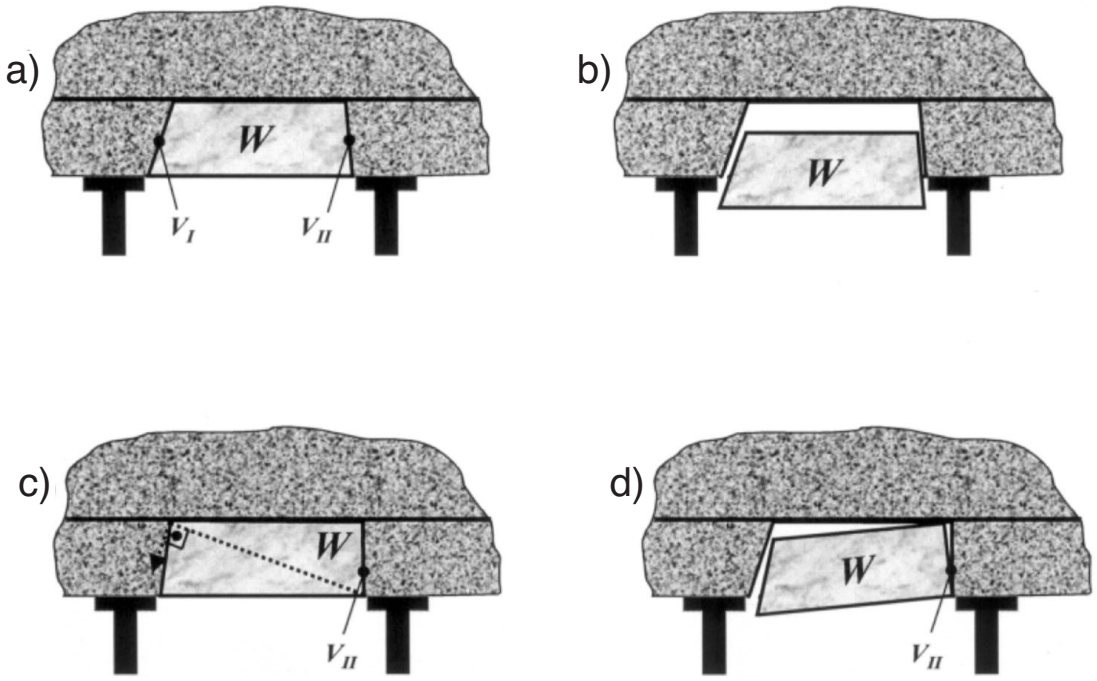

Figure 21—Schematic diagrams showing possible failure modes due to shear at discontinuity interfaces:
a) Keyblock is stable as $V_I > {}^1/_2 W$ and $V_{II} > {}^1/_2 W$ (steep angles, high friction)
b) Keyblock shear failure as $V_I < {}^1/_2 W$ and $V_{II} < {}^1/_2 W$ (shallow angle, low friction)
c) Although $V_I < {}^1/_2 W$, the keyblock is stable as $V_{II} > {}^1/_2 W$ and no block rotation is possible
d) Keyblock is unstable as $V_I < {}^1/_2 W$ and block rotation is kinematically possible ($V_{II} > {}^1/_2 W$)

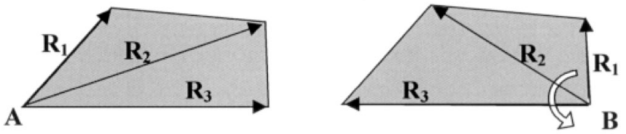

Rotation about A is not possible because R_2 is greater than R_3

Rotation about B is possible because R_1 and R_2 are both shorter than R_3

Figure 22—Principle of checking for possibility to rotate in two dimensions (after Esterhuizen[29])

Such a case is illustrated in Figure 21c. If, however, rotation is possible, failure will occur and the block will fall (Figure 21d).

The next task is to determine the criteria that prevent rotation. The ability of a keyblock to rotate depends on the geometry of the block and the pivot point. In this discussion, the corners of a keyblock that are inside the rock mass are called inner corners and the corners on the excavation surface are called surface corners.

In two dimensions, it is only possible for a keyblock to rotate if the radii from the pivot point to the inner corners of the block are shorter than the radius to the surface corner, as illustrated in Figure 22.

In three dimensions a similar method is followed. Each surface edge of a keyblock is considered as a possible candidate for rotation. Planes are constructed perpendicular to the edge of rotation through each inner corner of the block. Each plane represents a two dimensional section through the block. Each section is tested for rotation, using the two-dimensional test. If all the sections pass the test, the block cannot rotate about that edge. The principle is illustrated in Figure 23, where a section through one of the inner corners is shown.

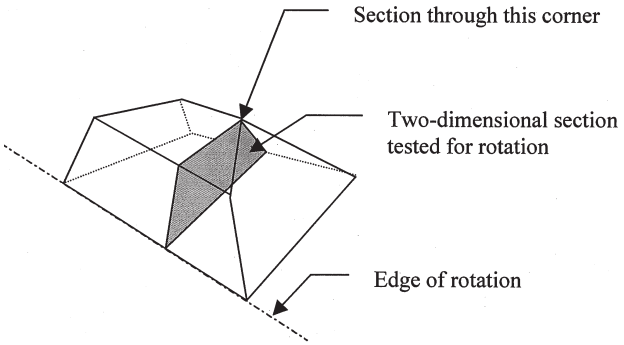

Figure 23—Sketch showing principle of testing for rotation about an edge (after Esterhuizen[29])

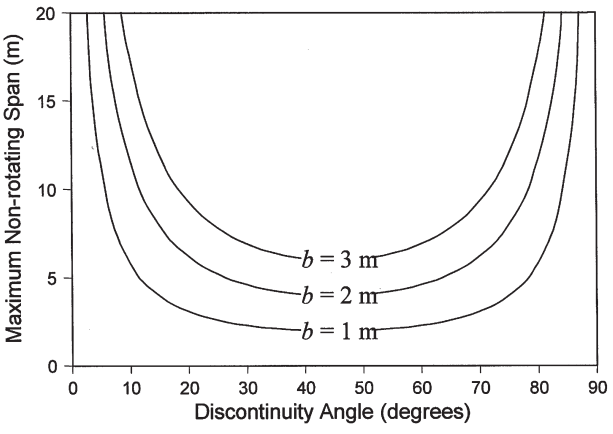

Figure 24—Upper limits of stable spans

A more mathematical description of the criteria that prevent rotation is presented by Daehnke *et al.*[22].

Figure 24 gives maximum non-rotating spans as a function of discontinuity angle and hangingwall beam thickness (b). It is evident that the upper bound of the span that will not rotate increases (for a fixed beam thickness) as the value of angle β (or α) departs, up or down, from 45 degrees. It is also noteworthy that for situations where b is greater than 2 m, rotation becomes an unlikely instability mechanism of the hangingwall. Conversely, kinematic rotation becomes increasingly possible for thinner hangingwall slabs.

In conclusion, the stability of keyblocks delineated by extension and shear fractures is dependent on buckling, shear and/or rotational failure mechanisms. When investigating the stability of keyblocks, the possibility of each of the three failure mechanisms needs to be considered. If the keyblock is unstable in any of the three failure modes, the unsupported span between adjacent support units needs to be decreased until neither buckling, shear nor rotational failure can occur.

SECTION 6

Quantifying zones of support influence

It is known that support units making up a support system can interact. Each support unit has a zone of influence around it, which might overlap with the zones of influence of adjacent support units. Understanding the zone of influence of a support unit can greatly assist in determining the correct support spacing when designing a support system.

The zone of support influence is defined as the *lateral extent* of the vertical *stress profile*, induced in the hangingwall beam by a loaded support unit. The zone of

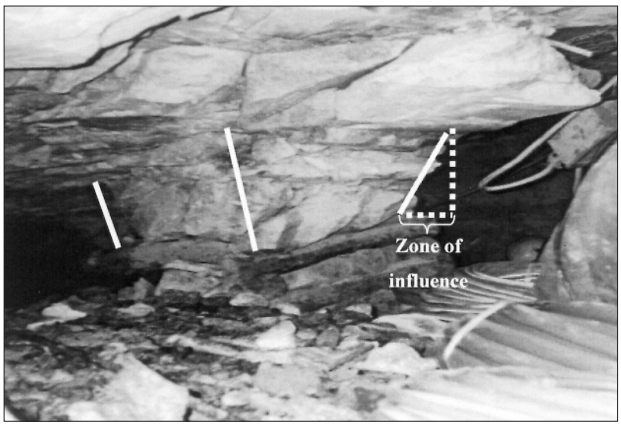

Figure 25—The zone of influence of a mat pack after a seismic event (courtesy Hartebeestfontein Gold Mine)

influence can extend some distance away from the immediate support-hangingwall contact, and hence can contribute towards rock mass stability between adjacent support units. A photograph illustrating the zone of influence of a pack following a rockburst is given in Figure 25, where it is apparent that the stabilizing influence of the pack has extended no more than an estimated 30 cm beyond the plan boundaries of the pack under the prevailing conditions.

The terms *stress profiles* and *lateral extent* are used in the definition of the zone of support influence. The *lateral extent* refers to the distance between the edge of the support unit and where the stress path intersects the bedding plane (See Figure 29). The *stress profile* refers to the stress distribution across the zone of influence. Zones of influence have some spatial distribution about the support unit, which describes the stress profile induced into the hangingwall by the support unit. The simplest spatial description of the stress profile associated with a zone of influence is in the form of a rectangular parallelepiped (i.e. rectangular box). This spatial description has been used in the past (Roberts[4]), where the extent of the zone of influence from the side of the support unit was typically taken as 1.0 to 1.5 m.

A review of a more detailed mathematical model (Daehnke *et al.*[30]) describing the zone of support influence in a discontinuous rock mass is given here. The following naming conventions are adopted to describe the basic parameters governing the zones of support influence.

Rock mass parameters:

- b = height of bedding plane above hangingwall skin
- φ = friction angle of bedding plane interface
- ϕ = friction angle of extension and shear fracture interfaces
- α = angle of extension fracture (measured from h/wall skin)
- β = angle of shear fracture (measured from h/wall skin)
- f = spacing of discontinuities such as shear fractures and joints.

Support parameters:

- F = support load
- r = radius of cylindrical support unit (e.g. elongate, prop)
- w = width of rectangular support unit (e.g. pack) = 2 r.

Zone of influence parameters:

- $\sigma(x)$ = zone of influence profile in two dimensions
- $\sigma(x,y)$ = zone of influence profile in three dimensions
- x = co-ordinate perpendicular to stope face
- y = co-ordinate parallel to stope face
- z = extent of zone of influence from support unit edge
- z_x = zone of influence extent extending in the x-direction from the support unit edge (3D case)
- z_y = zone of influence extent extending in the y-direction from the support unit edge (3D case).

Figure 26 shows a schematic in plan and section indicating some of the zone of influence parameters.

Homogeneous hangingwall beam

The simplest zone of influence model is associated with a

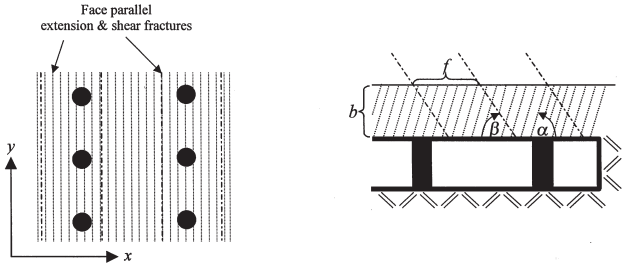

Figure 26—Naming conventions of rock mass parameters governing the zones of support influence (left—plan view; right—section view)

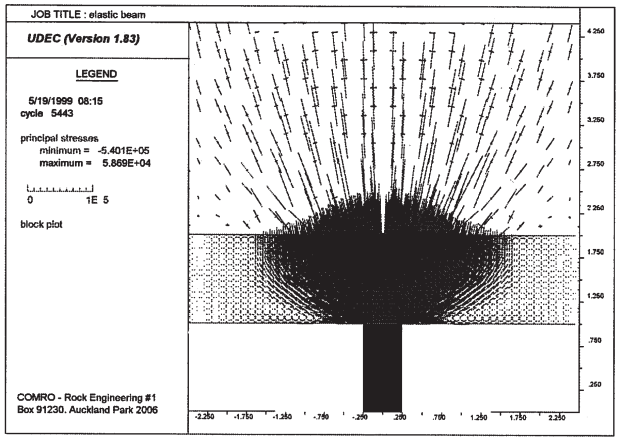

Figure 27—Principal stress trajectories through a homogeneous hangingwall beam loaded by a single support unit (b = 1.0 m, φ = 40°, F = 200 *kN*, w = 0.5 m)

homogeneous hangingwall beam, i.e. a continuous hangingwall beam not discretized by any discontinuities. The boundary element program UDEC (ITASCA[31]) was used to model the interaction of a single support unit (modelled as an elastic punch with a support load of 200 kN) with a homogeneous hangingwall beam (Figure 27).

For the purposes of this study, it will be shown that the maximum extent of the zone of support influence, z, is governed by the friction angle, φ, at the bedding plane interface and the bedding plane height, b. Note that in the model the bedding surfaces are represented by planes. This concept is schematically illustrated in Figure 28.

When the stress trajectories intercept the bedding plane at an angle exceeding the friction angle, slip occurs at the bedding plane. Slip at the lowest significant bedding plane

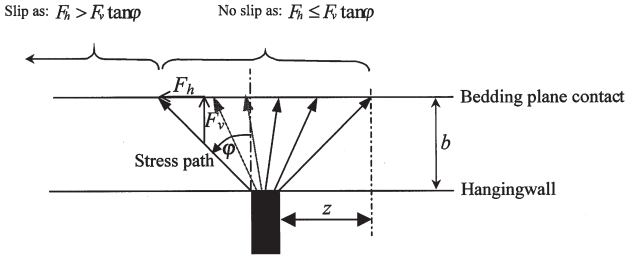

Figure 28—Maximum extent of the zone of support influence governed by bedding plane friction angle, φ, and bedding plane height, b

results in discontinuities (in the hangingwall beam and in the rock mass above the beam) opening, and comparatively little stress can be transferred across the bedding plane interface. This is a conservative assumption, as in reality bedding plane slip might be prevented due to compressive hangingwall stresses and the presence of comparatively large blocks of intact rock situated immediately above the bedding plane. The conservative engineering approach is, however, appropriate, as generally the presence and nature of discontinuities in the rock above the bedding plane are not well known. Hence, in all cases, support design and the interaction of adjacent support units should be based upon the *minimum* zones of influence.

Using the simplified model proposed in Figure 28, it follows that the zone of support influence extends for a distance of:

$$z = b \tan \varphi \qquad [16]$$

at the bedding plane contact.

The homogeneous beam model is applicable to shallow mines with comparatively competent and homogeneous hangingwall beams. In intermediate- and deep-level mines, however, extensive face-parallel mining-induced fractures fragment the hangingwall beam. As a consequence, zones of influence, in the direction normal to the discontinuities, can be of reduced extent. The homogeneous beam model can, however, approximate the zones of influence in the direction parallel to the discontinuities.

It is important to note that in many of the Figures that follow in this section, the stress distribution associated with the zone of support influence at the bedding plane is shown, and not the actual spatial distribution of the zone of influence (Figure 29).

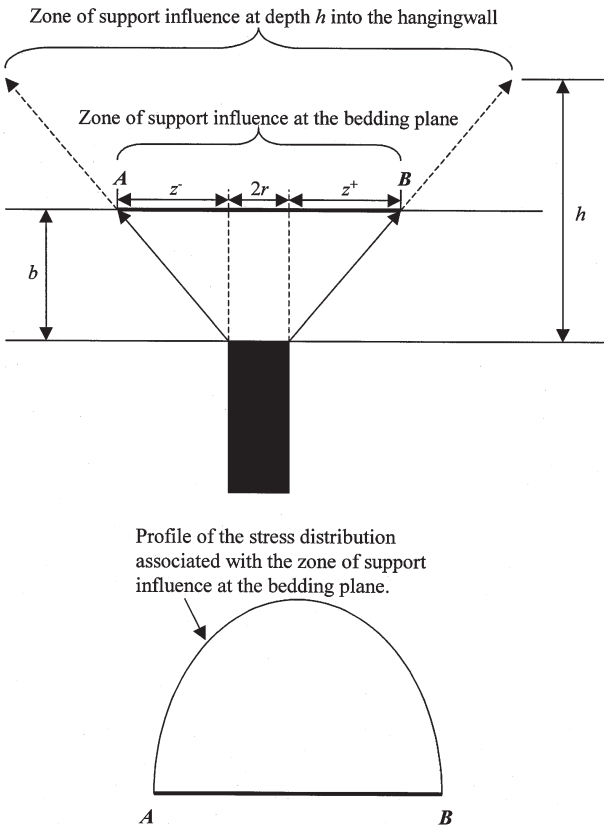

Figure 29—Schematic indicating the difference between the actual zone of influence and the stress profile associated with the zone of influence at a particular depth into the hangingwall

Numerical models of the homogeneous hangingwall beam are used to quantify the vertical stress profile (induced by the support unit) at the bedding plane interface. Figure 30 shows the numerically calculated vertical stress distribution at the interface, based on a two-dimensional plane strain model. The support resistance is calculated for a support unit, w = 0.5 m wide, and carrying a load of F = 200 kN. The friction angle at the interface is taken as φ = 40°. Also shown is a mathematical approximation of the numerically determined profile.

The mathematical function describing the zone of influence stress distribution is a parabola. The suitability of numerous functions (conical, hyperbolic, Gaussian) was evaluated, and the parabolic distribution was ultimately deemed to be the most appropriate and convenient function to describe stress profiles associated with zones of influence. In two dimensions the stress profile is mathematically described by:

$$\sigma(x) = \begin{cases} 0, & |x| > \zeta \\ \dfrac{3F}{4\zeta}\left[1 \pm \left(\dfrac{x}{\zeta}\right)^2\right], & |x| \le \zeta \end{cases}, \qquad [17]$$

where: $\zeta = z + r$ for cylindrical support units,
$\zeta = z + 0.5w$ for rectangular support units,

and, as defined before,

$$z = b\tan\varphi \cdot \qquad [18]$$

It is important to ensure that, for all stress profiles,

$$\int_{-\zeta}^{\zeta} \sigma(x)dx = F, \qquad [19]$$

i.e. the load at the support-hangingwall contact is equal to the total load within the zone of influence stress profile.

The three-dimensional formulation of the zone of influence in a homogeneous hangingwall beam follows analogous to the two-dimensional formulation. The zone of influence stress distribution in a homogeneous hangingwall beam is described by a circular paraboloid, i.e.

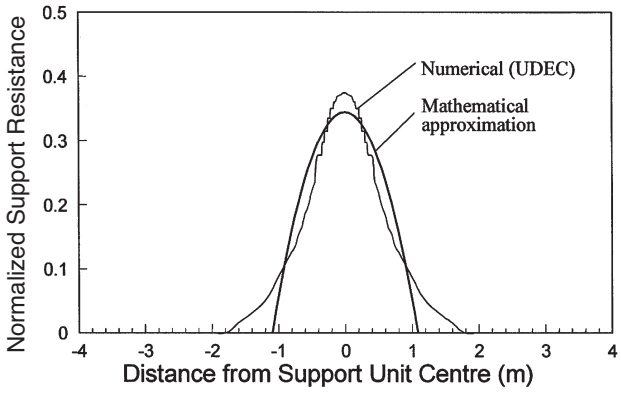

Figure 30—Numerical versus approximated support resistance profile. The normalized support resistance is defined as σ (x) / F

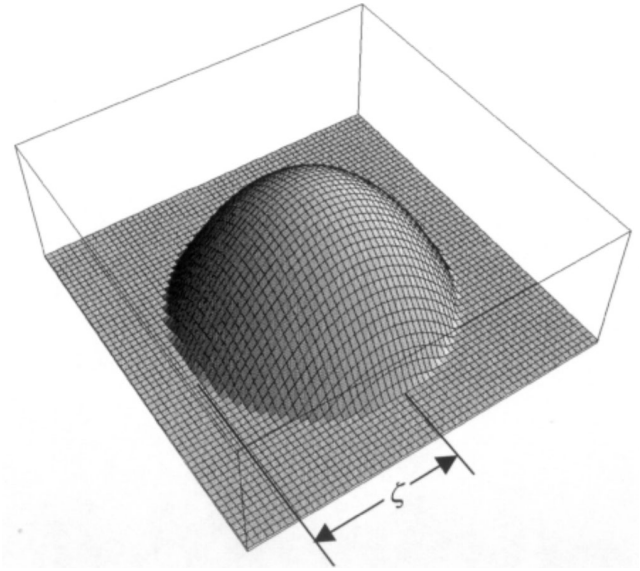

Figure 31—Zone of influence stress profile within a homogeneous beam in the shape of a circular paraboloid

$$\sigma(x,y) = \begin{cases} 0, & \left(\frac{x}{\zeta}\right)^2 + \left(\frac{y}{\zeta}\right)^2 > 1 \\ \frac{2F}{\pi\zeta^2}\left[1 - \left(\frac{x}{\zeta}\right)^2 \pm \left(\frac{y}{\zeta}\right)^2\right], & \left(\frac{x}{\zeta}\right)^2 + \left(\frac{y}{\zeta}\right)^2 \le 1 \end{cases} . \quad [20]$$

Figure 31 shows a three-dimensional carpet plot of $\sigma(x,y)$, where $\zeta = r + b \tan\varphi$.

Unclamped hangingwall beam fragmented by discontinuities

Numerical UDEC models were used to investigate zone of influence profiles in a hangingwall discretized by discontinuities. In intermediate- and deep-level mines, the hangingwall is typically fragmented by steeply dipping, closely spaced extension fractures. These generally terminate on bedding surfaces and are typically oriented parallel to the stope face.

Figure 32 shows the principal stress paths as calculated by UDEC for a hangingwall divided by individual sets of fractures dipping between 30° and 90°. In these models, no horizontal clamping stresses were applied to the hangingwall beam.

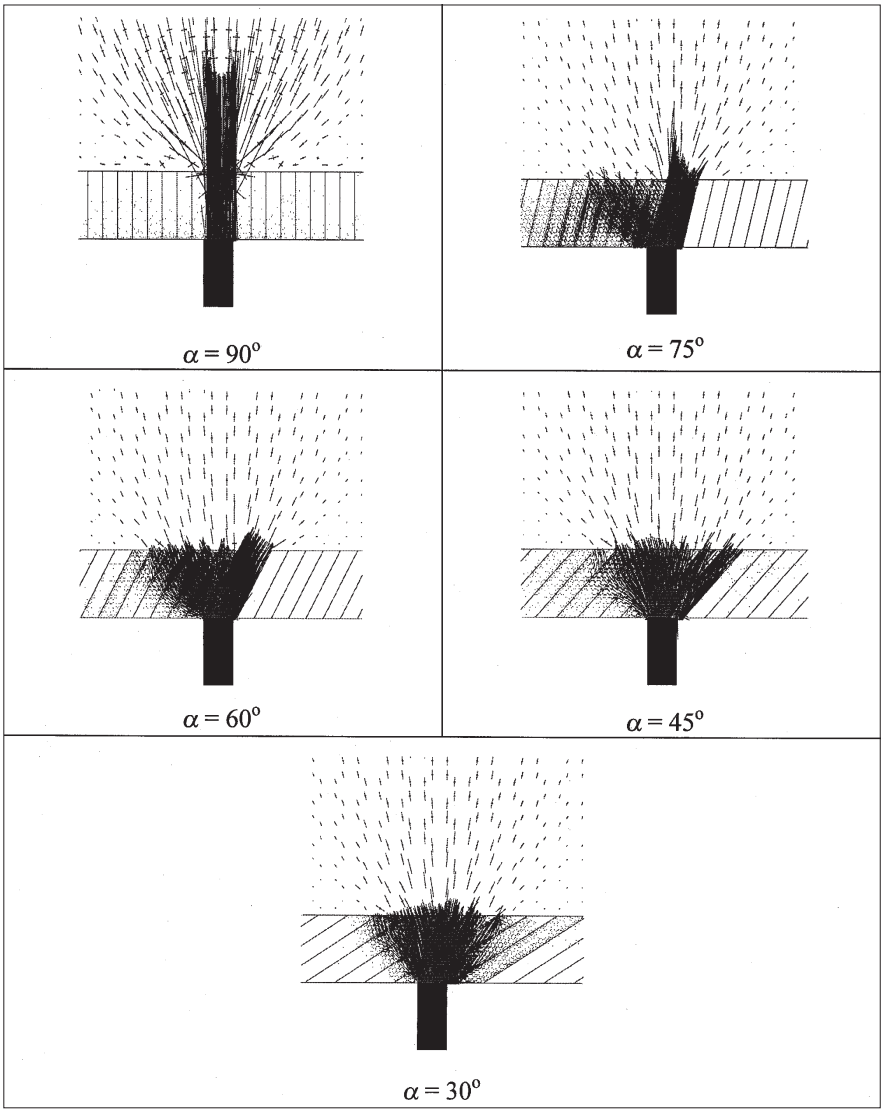

Figure 32—Principal stress paths through a hangingwall beam fragmented by extension fractures with dips of 30, 45, 60, 75 and 90 degrees

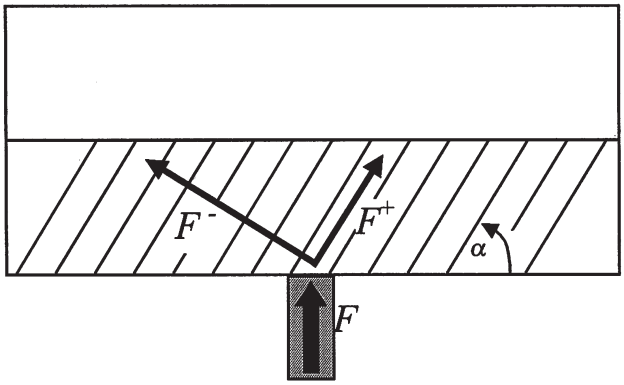

Figure 33—Idealized force trajectories through a hangingwall beam divided by extension fractures

It is apparent from Figure 32 that the stress trajectories follow two principal paths, i.e. (i) parallel to the discontinuities, and (ii) roughly perpendicular to the discontinuities. Figure 33 shows a schematic illustrating the two principal force vectors.

The zones on either side of the support unit differ. In an unclamped hangingwall beam, the zones of influence associated with F^+ and F^- are, respectively:

$$z^+ = \frac{b}{\tan\alpha} \quad \text{and} \quad z^\pm = b\tan\varphi. \qquad [21]$$

The value of z^+ cannot exceed z^- and, if $90°-\alpha > \varphi$, then $z^+ = z^-$.

Solving for the force vectors, it can be shown that,

$$F^+ = F\sin\alpha \quad \text{and} \quad F^\pm = F\cos\alpha. \qquad [22]$$

The vertical components of forces F^+ and F^- are

$$F_v^+ = F\sin^2\alpha \quad \text{and} \quad F_v^\pm = F\cos^2\alpha. \qquad [23]$$

Thus, the ratio of F_V^+ versus F_V^- is equal to $\tan^2\alpha$. As the fracture angle, α, tends to 90°, F_V^- reduces to zero. The corresponding zone of influence, z^-, needs to be modified accordingly, and when $\alpha = 90°$, $z^- = 0$. In this study, the following correction function is applied to z^-:

$$z^\pm = b\tan\varphi\frac{100}{\left(100+\tan^2\alpha\right)}. \qquad [24]$$

Figure 34 shows zone of influence stress profiles for α = 90°, 60° and 30°.

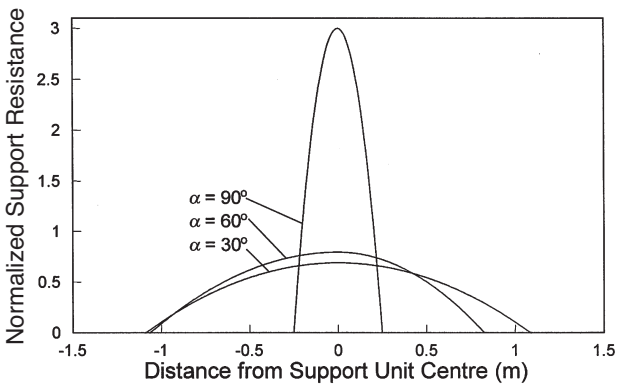

Figure 34—Zone of influence stress profiles for α = 90°, 60° and 30°

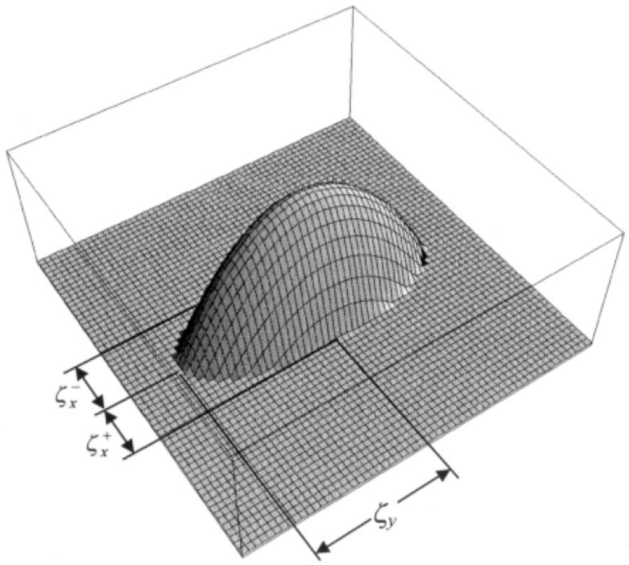

Figure 35—Zone of influence stress profile within an unclamped hangingwall discretised by vertical discontinuities striking parallel to the *y*-direction (i.e. parallel to the face)

In the two-dimensional formulation, it was shown that the zones of influence on either side of the support unit differ when the hangingwall is fragmented by discontinuities. Figure 35 shows the zone of influence profile for a hangingwall beam transected by vertical discontinuities, where:

$$\zeta_y = r + b\tan\varphi, \qquad [25]$$

$$\zeta_x^+ = \zeta_x^\pm = r. \qquad [26]$$

Figure 36 shows a three-dimensional view of the stress profile associated with the zone of influence in a hangingwall discretized by oblique discontinuities. The hangingwall is assumed to be unclamped. The general stress profile, describing the zone of influence within an unclamped hangingwall beam, is given by Equation [27].

$$\sigma(x,y) = \begin{cases} 0, \ \left(\frac{x}{\zeta_x^\pm}\right)^2 + \left(\frac{y}{\zeta_y}\right)^2 > 1 \ \ \& \ \ x \le 0 \\ \Omega\left[1-\left(\frac{x}{\zeta_x^\pm}\right)^2 - \left(\frac{y}{\zeta_y}\right)^2\right], \ \left(\frac{x}{\zeta_x^\pm}\right)^2 + \left(\frac{y}{\zeta_y}\right)^2 \le 1 \ \& \ x \le 0 \\ \Omega\left[1-\left(\frac{x}{\zeta_x^+}\right)^2 - \left(\frac{y}{\zeta_y}\right)^2\right], \ \left(\frac{x}{\zeta_x^+}\right)^2 + \left(\frac{y}{\zeta_y}\right)^2 \le 1 \ \& \ x \ge 0 \\ 0, \ \left(\frac{x}{\zeta_x^+}\right)^2 + \left(\frac{y}{\zeta_y}\right)^2 > 1 \ \ \& \ \ x \ge 0 \end{cases} \qquad [27]$$

$$\text{where:} \quad \Omega = \frac{4F}{\pi\zeta_y\left(\zeta_x^+ + \zeta_x^\pm\right)}, \ \text{and} \qquad [28]$$

$$\zeta_y = r + b\tan\varphi, \qquad [29]$$

$$\zeta_x^+ = r + \frac{b}{\tan\alpha}, \qquad [30]$$

$$\zeta_x^\pm = r + b\tan\varphi\frac{100}{100+\tan^2\alpha}. \qquad [31]$$

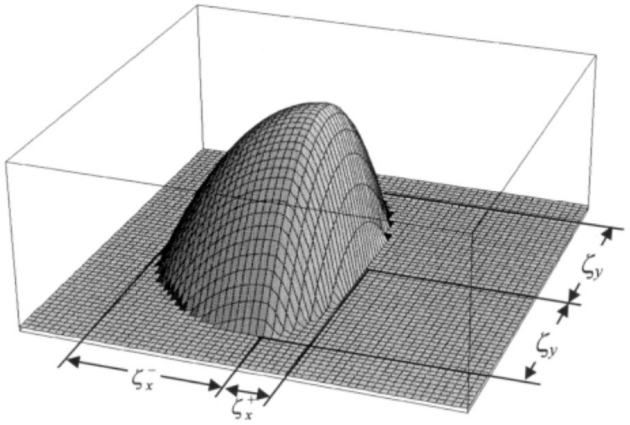

Figure 36—Zone of influence stress profile within an unclamped hangingwall discretized by oblique discontinuities

Clamped hangingwall beam fragmented by discontinuities

In intermediate- and deep-level mines, fracturing ahead of the stope face induces rock dilation leading to compressive hangingwall stresses parallel to the skin of the excavation (Jager and Roberts[12]). Compressive hangingwall stresses usually contribute significantly to the rock mass stability. Squelch[33] measured maximum compressive hangingwall stresses of 1 to 10 MPa at depths between 0.7 and 2.2 m into the hangingwall in a backfilled stope. These horizontal stresses clamp the fractured rock together and, depending on the orientation of the fractures, can significantly improve the structural integrity and stability of the hangingwall (Jager and Roberts[12]).

Herrmann[34] found that in stopes with back area caving, stress relaxation occurred in the lower layers of the hangingwall, and noted the importance of rock confinement to maintain compressive hangingwall stresses. Rockfalls and caving in the back area generally lead to reduced hangingwall confinement. However, compressive hangingwall stresses can still be maintained when frictional resistance, generated at bedding surfaces, restricts the lateral hangingwall movement.

Compressive hangingwall stresses affect the zone of influence by clamping hangingwall discontinuities together. As a consequence, support stresses can be transmitted obliquely across discontinuities, and the zone of influence is extended to either side of the support unit. To quantify the stress profile and extent of the zone of influence associated with a clamped hangingwall beam, the simplified analytical model shown in Figure 37 is considered.

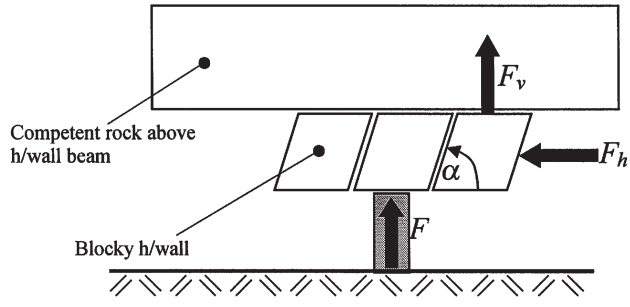

Figure 37—Simplified model used to quantify the zone of support influence in a clamped, discontinuous hangingwall beam

By resolving the forces F_h and F_v normal and parallel to the inclined fracture, it can be shown that the maximum vertical force, F_v, that can be transmitted by a hangingwall block, adjacent to the block supported directly by the support unit, is:

$$F_v = F_h \frac{\mu \pm \cot\alpha}{1 + \mu\cot\alpha}, \qquad [32]$$

where $\mu = \tan\ \phi$, and ϕ is the friction angle of the inclined fracture interface. Note that, due to the interlocking nature of *in situ* mining-induced fractures, the associated effective friction angle is typically comparatively high, and values of $\phi = 50°$ to $\phi = 60°$ are considered realistic. For the two-dimensional plane strain case $F_h = b\ \sigma_h$. The minimum stress, σ_h^{crit}, that is required to clamp the hangingwall discontinuities, is calculated by setting $F_v = F\ \sin^2\alpha$ (from Equation [23]), i.e.

$$\sigma_h^{crit} = \frac{F}{b}\chi \text{ and } \chi = \frac{\sin^2\alpha\left(1 + \mu\cot\alpha\right)}{\mu \pm \cot\alpha}. \qquad [33]$$

The function χ is graphically illustrated in Figure 38 for interface friction angles of $\phi = 50°$ and $\phi = 60°$. If, for example, $b = 1.0$ m, $\phi = 50°$ and $\alpha = 60°$, then $\sigma_h^{crit} = 2.1\ F$. For a typical elongate load of $F = 200$ kN, this implies that the horizontal compressive stresses should be at least $\sigma_h = 0.42$ MPa for the discontinuities to be sufficiently clamped that the zones of influence correspond to the zones in a homogeneous hangingwall beam. This is an important and positive insight, as it implies that in intermediate- and deep-level mines, where typically $\sigma_h > 1.0$ MPa, the zones of influence in a hangingwall fragmented by moderately to steeply dipping fractures can generally be accurately approximated by the corresponding zones in homogeneous beams.

Using an analogous approach to the two-dimensional case, it can be shown that in three dimensions (assuming an isotropic horizontal stress in the hangingwall), considering that

$$F_h = \frac{4}{3}\zeta_y b\sigma_h, \qquad [34]$$

the minimum stress, σ_h^{crit}, that is required to clamp the hangingwall discontinuities, is:

$$\sigma_h^{crit} = \frac{3F}{4b\zeta_y}\ x \text{ and, as before, } x = \frac{\sin^2\alpha\left(1 + \mu\cot\alpha\right)}{\mu - \cot\alpha}. \qquad [35]$$

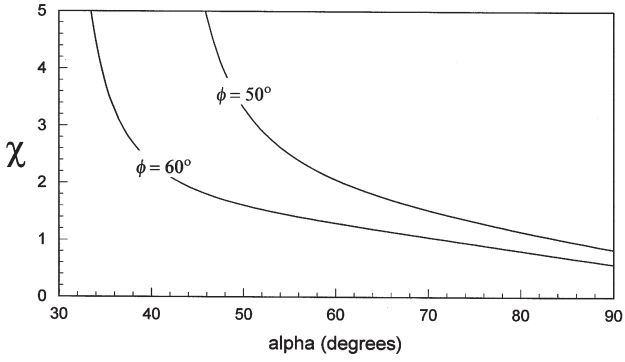

Figure 38—Graphical illustration of function χ for $\phi = 50°$ and $\phi = 60°$

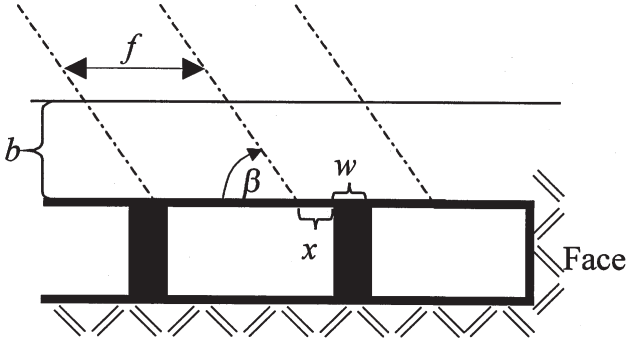

Figure 39—Hangingwall beam discretized by shear fractures (Daehnke *et al.*[30])

As noted before, it is evident from Equation [35] that comparatively low hangingwall clamping stresses are required, such that the zones of influence in a discontinuous hangingwall beam correspond to the zones of influence within a homogeneous hangingwall beam.

Effect of shear fractures on the zone of support influence

A probabilistic approach is used to quantify the effect of shear fractures on the zone of support influence. Consider a hangingwall beam fragmented by shear fractures, oriented at an angle, β, as shown in Figure 39. It is assumed that the fractures are not clustered in any way (although this can happen in certain circumstances). Hence, they have an equal probability of being located at any point on the hangingwall along the strike direction. All arguments that follow assume uniformly distributed fractures.

The parameters which are considered in the probabilistic formulation are:

- w = support width (rectangular support units, e.g. packs)
- r = radius of support (cylindrical support units, e.g. props)
- x = distance from the edge of the support to the fracture
- f = fracture spacing (constant).

The shear fractures are randomly distributed in relation to the support units, i.e. the distance, x, is not constant. The minimum value of x is 0, when the fracture coincides with the support edge. This is considered the worst case as, with no clamping stresses, the zone of support influence could be limited by the shear fracture. Conversely, the best case is assumed to occur when $x = f - r$, which is taken as the maximum value of x (i.e. when the adjacent fracture is situated immediately above the support unit centre). At $x > f - r$, the effective stress transfer from the support unit to the hangingwall is assumed to be compromised by the adjacent shear fracture, and the zone of influence is potentially once again limited by the shear fracture.

It has just been established that a fracture can be situated anywhere between the support unit and a distance $f - r$ from the support unit, thus x can take on any value between 0 and $f - r$. Consider a point, which is situated a fixed distance, d, from the support unit A (Figure 40). The probability that the fracture is located within this distance d from support unit A,

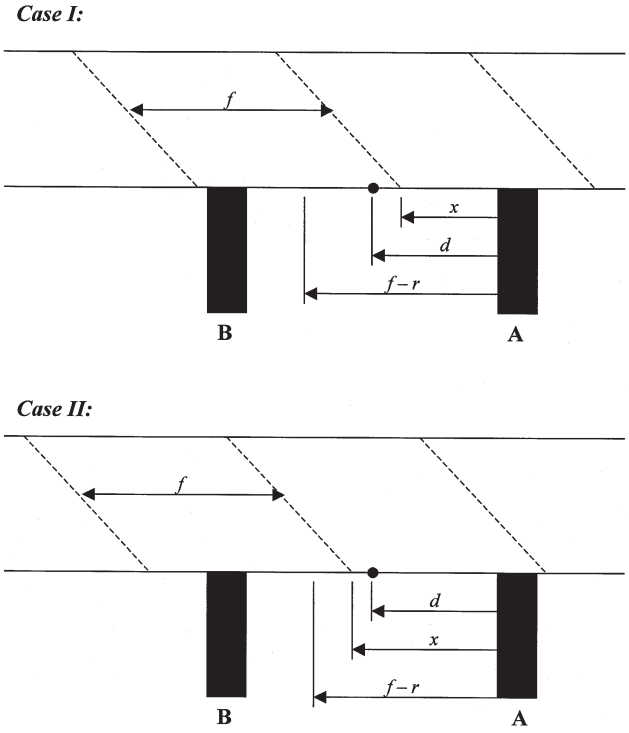

Figure 40—Two possible locations of the fracture set relative to the support units are shown here

or in other words, the probability that d is equal to or exceeds x (Case I in Figure 40), is given by

$$P_{d \geq x} = \begin{cases} \dfrac{d}{f-r} & \text{if } 0 \leq d \leq f-r \\ 1 & \text{if } d > f-r \end{cases} \quad [36]$$

The probability that x will exceed d (Case II in Figure 40), is given by

$$P_{x \geq d} = 1 - P_{d \geq x} = 1 - \left(\frac{d}{f-r}\right). \quad [37]$$

It is thus possible to determine d probabilistically

$$d = P_{d \geq x}(f-r) = (1 - P_{x>d})(f-r). \quad [38]$$

For example, if $P_{x>d} = 0.8$ (i.e. the probability is 80 per cent that the fracture is not within a distance, d, of the support edge), then

$$d = (1 - 0.8)(f-r) = 0.2(f-r).$$

If no horizontal compressive stress acts on the beam, i.e. $\sigma_h = 0$, then the extent of the zone of influence, on the left hand side of the support, z_x^-, is given by:

$$z_x^- = \begin{cases} \dfrac{b}{\tan\beta} + d, & \beta > \dfrac{\pi}{2} - \varphi \\ b\tan\varphi, & \beta \leq \dfrac{\pi}{2} - \varphi \end{cases} \quad [39]$$

Substituting Equation [38] in [39] gives:

$$z_x^- = \begin{cases} \dfrac{b}{\tan\beta} + (1-P)(f-r), & \beta > \frac{\pi}{2} - \varphi \\ b\tan\varphi, & \beta \leq \frac{\pi}{2} - \varphi \end{cases} \quad [40]$$

Note that on the left hand side of the support the stress trajectories are oriented normal to the extension fractures,

thereby clamping the fractures. Hence the ubiquitous presence of the extension fractures does not affect the zone of influence z_x^-. To avoid being too conservative in the design of support spacing, it may be beneficial to assume that P = 0.9. This gives

$$d = (1 - 0.9)(f - r) = 0.1(f - r). \quad [41]$$

If the horizontal compressive stress, σ_h, is high enough to ensure that the beam is clamped, the extent of the zone of influence on the left hand side of the support, z_x^-, is given by $z_x^- = b\tan\varphi$. The above arguments are used in the next section to quantify the zones of influence in intermediate- and deep-level mines.

Quantifying zones of support influence in intermediate- and deep-level mines

The aim of this section is to briefly review the zones of influence applicable to intermediate- and deep-level mines. The typical hangingwall of mines at these depths is characterized by face parallel, ubiquitous and closely spaced extension fractures, with face-parallel conjugate shear fractures spaced between 1 m and 3 m.

Table III is given to summarize the principal equations and facilitate the convenient quantification of zones of support influence. Note that the maximum value of z_x^- cannot exceed $b\tan\varphi$, even if β is greater than $\pi/2 - \varphi$. Assuming an elliptic parabolic stress distribution (Equation [27]) about the support, the maximum stress can be calculated using the following equation:

$$\sigma_{max} = \frac{4F}{\pi\zeta_y\left(\zeta_x^+ + \zeta_x^-\right)}, \quad [42]$$

$$\text{where:} \quad \zeta_{x,y}^{+,-} = z_{x,y}^{+,-} + r. \quad [43]$$

Quantifying the zone of influence of the stope face in intermediate- and deep-level mines

A preliminary investigation into the zone of influence of the stope face was carried out by Daehnke *et al.*[30]. The boundary element code, UDEC, was used to model the influence of the stope face and these results were used to facilitate the formulation of analytical models.

From the numerical modelling results, it was clear that the orientation of the extension fractures has a pronounced influence on the stress path at the stope face. However, investigations into the zones of *support* influence showed that in most intermediate- and deep-level mines, the horizontal stresses are high enough to clamp the fragmented hangingwall beam (see Section 6, Equation [35]). The horizontal stress is hence assumed to be sufficient to clamp the hangingwall beam ($\sigma_h > \sigma_h^{crit}$), and thus

$$z = b\tan\varphi. \quad [44]$$

For the purpose of this analysis, a linear decline in stress with distance from the face is assumed. A further assumption, which is realistic for deep stopes (Ryder[35]), is that the face rock is heavily fractured for about 1 m into the face, and therefore the vertical stress 1 m into the face is approximately equal to the UCS of the face rock (see Figure 41). It is recognised that this is only an approximation of the stress distribution at the face and detailed inelastic numerical modelling is required to obtain a more accurate stress distribution. In order to estimate the zone of influence of the stope face, however, an approximate stress distribution is adequate.

The zone of influence stress distribution of the stope face is described by:

$$\sigma(x,y) = \begin{cases} \frac{\sigma_c}{1+z}(z - x) & ;\ 0 \le x \le z \\ 0 & ;\ x > z \end{cases} \quad [45]$$

where: σ_c = UCS of the face rock
x = distance measured from the edge of the face, and
z = the extent of the zone of influence from the edge of the face = b tan φ.

Quantifying the zone of influence of the stope face in shallow mines

In shallow mines, the hangingwall is generally characterized by low or no clamping stresses, and is discretized by

Table III

Zones of influence in intermediate- and deep-level mines

Is $\sigma_h > \sigma_h^{crit}$? (Equation [35])	
Yes	No
↓	↓
Clamped	**Unclamped**
$z_x^+ = b\tan\varphi$	$z_x^+ = \begin{cases} \frac{b}{\tan\alpha} & \text{if } \alpha > \frac{\pi}{2} - \varphi \\ b\tan\varphi & \text{if } \alpha \le \frac{\pi}{2} - \varphi \end{cases}$
$z_x^- = b\tan\varphi$	$z_x^+ = \begin{cases} \frac{b}{\tan\beta} + (1-P)(f-r) & \text{if } \beta > \frac{\pi}{2} - \varphi \\ b\tan\varphi\,\frac{100}{100+\tan^2\alpha} & \text{if } \beta \le \frac{\pi}{2} - \varphi \end{cases}$
$z_y = b\tan\varphi$	$z_y = b\tan\varphi$

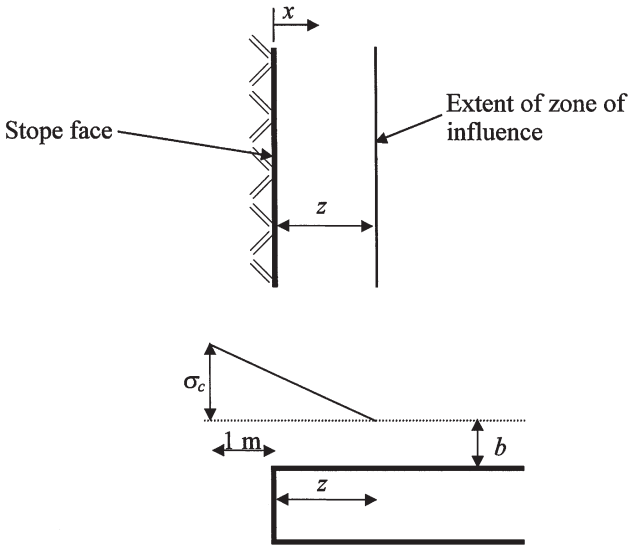

Figure 41—Zone of stope face influence and associated stress distribution

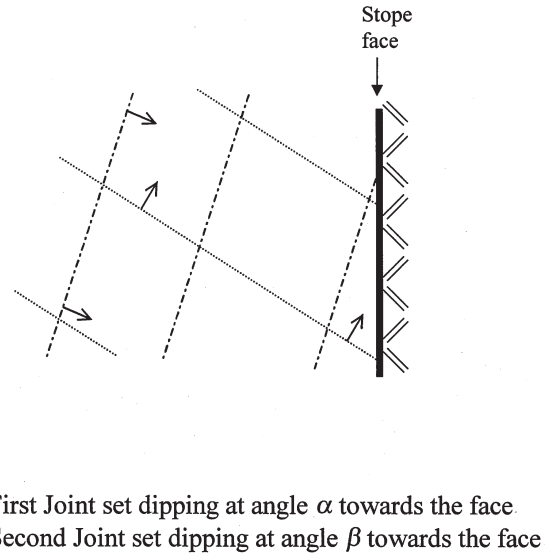

Figure 42—Joint sets associated with a stope face in a shallow mining environment

conjugate joint sets. Consider a stope as shown in Figure 42. The hangingwall is intersected by two joint sets oriented at two different angles with respect to the stope face. The dip direction of the joint sets is indicated in Figure 42.

As can be seen from Figure 42, the joints intersect the stope face. Due to the absence of horizontal clamping stresses in shallow mines, the zone of influence of the stope face will be limited to the block delineated by these joints. Thus, in shallow mines, the zones of influence are controlled by intersecting joint sets. Generally there are insufficient horizontal stresses to clamp adjacent blocks, and therefore the blocks need to be supported individually.

The determination of the exact shape of the zone of influence of the stope face and the associated stress distribution is a complex problem, and has not been fully addressed as yet. In the interim, the zone of influence of the stope face in shallow mines should conservatively be assumed to be zero.

Quantifying the zone of influence of backfill

A preliminary study to investigate the zone of influence of backfill was undertaken by Daehnke *et al.*[30]. The boundary element code, UDEC (ITASCA[31]), was used to model the influence of backfill, and the results obtained in this way were used to facilitate the formulation of analytical models.

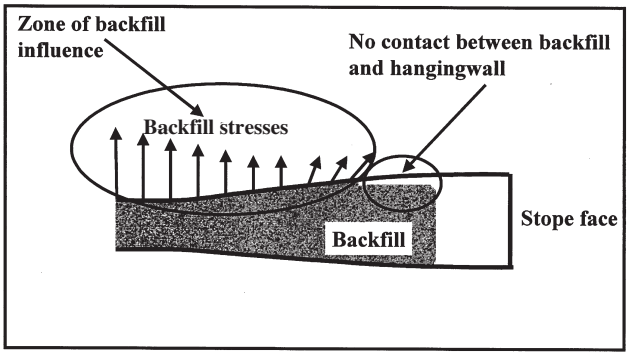

Figure 43—Graphical representation of the backfill – hangingwall contact zone (section on strike)

The numerical analyses indicated that the zone of backfill influence does extend ahead of the point of backfill-hangingwall contact. However, from underground observations it was found that the point of contact between the backfill and the hangingwall is typically 0.5 m to 1 m behind the backfill edge. A graphical representation of the zone of backfill influence and the lack of backfill-hangingwall contact in the immediate vicinity of the backfill face, is given in Figure 43.

Assuming the backfill is in contact with the hangingwall at the edge of the backfill, the zone of backfill influence can be expressed as:

$$z = b\tan\varphi, \qquad [46]$$

where b is the bedding thickness and φ is the friction angle of the bedding plane contact. A parameter c is defined as the average distance between the edge of the backfill and the point of contact between the hangingwall and backfill. Thus, the effective zone of influence of the backfill, z_b, is the difference between z and c.

$$z_b = z - c, \qquad [47]$$

$$z_b = b\tan\varphi - c. \qquad [48]$$

For example, consider a bedding surface 1 m above the hangingwall surface with an interface friction angle of 45°. If the value of c for the panel in which the backfill is placed is 50 cm, the effective zone of influence of the backfill is:

$$z_b = 1\text{ m} - 0.5\text{ m} = 0.5\text{ m}. \qquad [49]$$

Thus, the zone of influence of the backfill would extend approximately 50 cm ahead of the backfill face.

The zone of influence of backfill is assumed to be zero if it does not take any load, i.e. immediately after installation of the backfill. Note that in practice the value of c is increased by the further distance of backfill-hangingwall contact required to generate a significant support resistance (e.g. 100 kN/m^2). This distance depends on backfill quality, closure rate and stoping width.

SECTION 7

A unified engineering approach to quantify stable hangingwall spans of hangingwalls with face-parallel fractures

An engineering approach to quantify stable spans of discontinuous hangingwalls is proposed. The approach makes use of models and support design methodologies described in Sections 5 and 6. In essence, the approach combines the zones of support influence with the hangingwall stability controlled by buckling, rotating and shearing keyblocks. This design tool is of practical value and enables the rock engineer to make initial designs of appropriate support spacing by using a few comparatively straightforward graphs.

It is emphasized, however, that certain assumptions are made during the design process. To ensure rock mass stability and reduce rock-related hazards, these assumptions are generally conservative, i.e. the resulting support system is marginally over-designed, providing some factor of safety.

Figure 44—Example of a hangingwall with FPFs

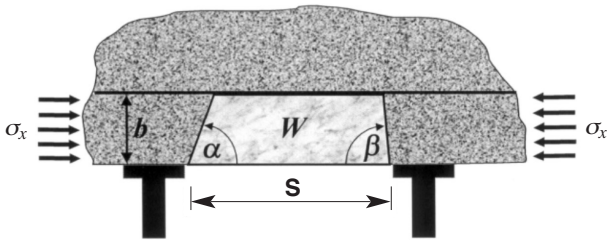

Figure 45—Critical keyblock parameters influencing the rock mass stability

To fully optimize the support system, it is recommended that the complete models developed by, specifically, SIMRAC projects GAP330, GAP335 and GAP627 be applied. It is further recommended that appropriate software, such as SDA II (CSIR[32]), be used to expedite the more accurate evaluation of support systems.

Combining zones of influence with keyblock stability

The tributary area requirements reviewed in the previous sections are adequate to address general stability requirements of a continuous, unfractured hangingwall beam. In practice, however, the hangingwall is fragmented by joints and mining-induced fractures. In a highly discontinuous hangingwall, the tributary area criteria may not ensure rock mass stability between adjacent support units.

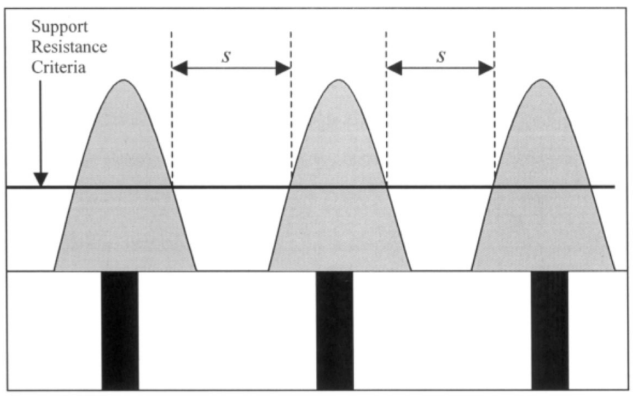

Figure 46—Cross-section of support resistance profiles, illustrating the unsupported sections (s), which have to be checked for keyblock stability

In this section, the stability criteria of a hangingwall with FPFs (face parallel fractures) are developed. The failure of hangingwalls with FPFs is generally characterized by keyblock failure (sliding and rotational failure) and beam buckling. An example of a hangingwall with FPFs is given in Figure 44.

The work conducted as part of SIMRAC projects GAP330 (Daehnke *et al.*[5]) and GAP627 (Daehnke *et al.*[30]) quantified the rotational, sliding and buckling stability envelopes of hangingwall keyblocks. It was found that the stability is predominantly governed by the keyblock height (b) and the angles of the discontinuities discretizing the keyblock, α and β (see Figure 45). In intermediate and deep level mines, the angles α and β are normally defined by face-parallel mining-induced extension and shear fractures respectively.

It was further found that the compressive hangingwall stresses contribute towards the hangingwall stability. In the design method proposed here, a compressive stress of σ_x = 1 MPa is assumed. In deep level mines σ_x might exceed 1 MPa, however, until further *in situ* measurements have been made, σ_x = 1 MPa is considered an appropriately conservative assumption for the purposes of designing support systems.

A cross-section of zones of support influence is shown in Figure 46, also indicating the support resistance criteria. Where the support resistance profile (zone of influence) falls beneath the support resistance criteria, the effect of the zone of influence is ignored (a conservative assumption). The length of this distance is denoted by s. This unsupported section must now be analysed further to check for buckling, rotational and shearing keyblock stability (as discussed in Section 5).

Support spacing requirements for rockfall conditions and hangingwalls with face-parallel fractures (FPFs)

Figure 47 gives stability envelopes of keyblocks based on instability height (b), support force (F), unsupported span (s), discontinuity angles (α and β), and γ, where γ = 90° – ϕ and ϕ is the apparent friction angle associated with the fracture surfaces. Due to the interlocking and matching surfaces of mining-induced fractures, the apparent friction angle (ϕ) is relatively high, and values of 50° to 60° are considered realistic.

Two main stability zones are given in Figure 47:

- ***Dark grey zone:*** Here the keyblocks are bounded by shallow dipping fractures and keyblock rotation and subsequent sliding is likely. In this zone the stability of keyblocks is governed by overlapping zones of support influence, and the work conducted during SIMRAC project GAP627 (Daehnke *et al.*[30]) is applied to estimate maximum stable unsupported spans, whilst maintaining rock mass stability. In quantifying the extent of the zones of support influence, a bedding plane friction angle of 20° is assumed.
- ***Light grey zone:*** Relatively steeply dipping fractures reduce the possibility of block rotation and failure is generally governed by beam buckling. Note that in this case the zones of influence also contribute towards the hangingwall stability, and the maximum stable unsupported spans are consequently extended. The extent of this zone is dependent on the fractured

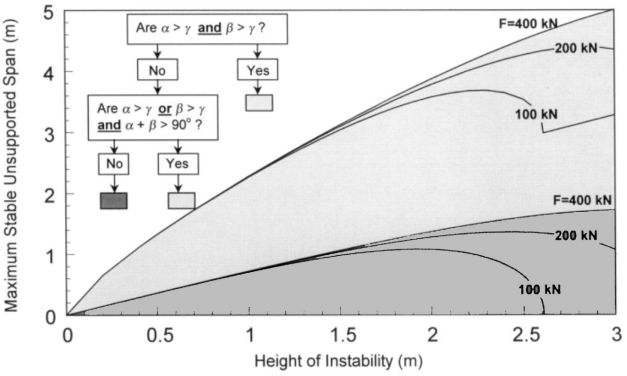

Figure 47—Rockfall stability envelopes for hangingwalls with FPFs as a function of instability height, unsupported span, support load and discontinuity orientation (γ = 90° – ϕ, where ϕ is the friction angle associated with the fracture surfaces)

hangingwall stiffness. Data from Bandis *et al.*[28] was used to estimate the stiffness of the fractured hangingwall (for further details see Daehnke *et al.*[5]). The *in situ* hangingwall beam stiffness should be quantified to *accurately* determine the extent of this zone. However, for the purposes of an engineering approach, the extent given here is considered representative for most underground rock mass conditions.

As an example, consider the stability of a hangingwall fragmented by face-parallel extension and shear fractures dipping at α = 50° and β = 30°, respectively and the friction angle is assumed to be ϕ = 50° (hence γ = 90°-50° = 40°).

Are $\alpha > \gamma$ **and** $\beta > \gamma$?	No
Are $\alpha > \gamma$ or $\beta > \gamma$ **and** $\alpha + \beta > 90°$?	No

Since $\alpha + \beta < 90°$, the dark grey stability zone is applicable (using the flowchart in Figure 47). Assuming a support unit load of F = 200 kN and height of instability b = 1.5 m, the maximum stable unsupported span is determined from Figure 47 as 1.0 m. Note that, by installing props with headboards, the unsupported span remains the same, but the prop spacing can be increased by the length of the load spreader.

If α = 60° and β = 80° and the friction angle is assumed to be ϕ = 50° (hence γ = 40°), the stability zone is determined by the light grey area. From Figure 47 the maximum unsupported span is given as 3.0 m (assuming F = 200 kN and b = 1.5 m).

It is emphasized that the above stability zones are simplified approximations of the stability envelopes developed as part of GAP330 and GAP627 (Daehnke *et al.*[5, 30]). To fully optimize the support systems, it is recommended that the SDA II software or the 3D stability plots given by Daehnke *et al.*[5,31] be used.

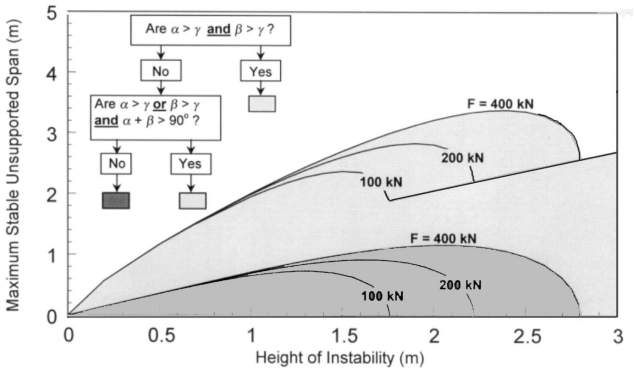

Figure 48—Rockburst stability envelopes for hangingwalls with FPFs as a function of instability height, unsupported span, support load and discontinuity orientation (γ = 90° – ϕ, where ϕ is the friction angle associated with the fracture surfaces)

Support spacing requirements for rockburst conditions and hangingwalls with face-parallel fractures (FPFs)

The stability requirements for rockburst conditions and hangingwalls with FPFs follow analogously to the rockfall case. The hangingwall is assumed to be accelerated to a velocity of 3 m/s, which is decelerated over a distance of 0.2 m. The extent of the zones of support influence is calculated for an effective hangingwall weight taking into account the rock mass deceleration.

Figure 48 gives the stability envelopes for rockburst conditions of a hangingwall with FPFs. As in the rockfall case, two stability zones (light and dark grey) are shown. The appropriate stability zone is dependent on the discontinuity angles (α and β) and friction angle (ϕ).

As an example, consider the stability of the same hangingwall, fragmented by face-parallel extension and shear fractures dipping at α = 50° and β = 30°, respectively and γ = 40°, as in the previous section.

Are $\alpha > \gamma$ **and** $\beta > \gamma$?	No
Are $\alpha > \gamma$ or $\beta > \gamma$ **and** $\alpha + \beta > 90°$?	No

Since $\alpha + \beta < 90°$, the dark grey stability zone is applicable (using the flowchart in Figure 48). Assuming a support unit load of F = 200 kN and height of instability b = 1.5 m, the maximum stable unsupported span is determined from Figure 48 as 0.9 m. (This is slightly less than for the rockfall case.) Note that, by installing props with headboards, the unsupported span can be made the same by increasing the prop spacing by the length of the load spreader.

Figure 49—Example of a blocky hangingwall

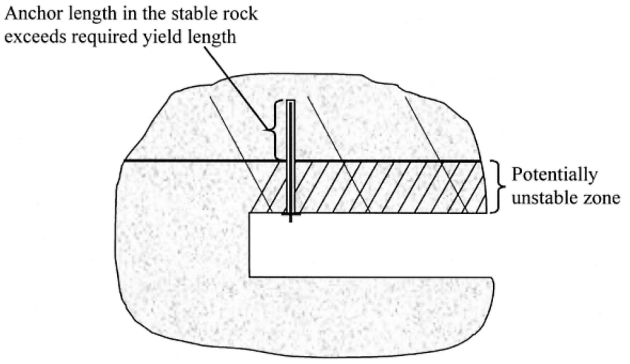

Figure 50—Length requirements of yielding tendons

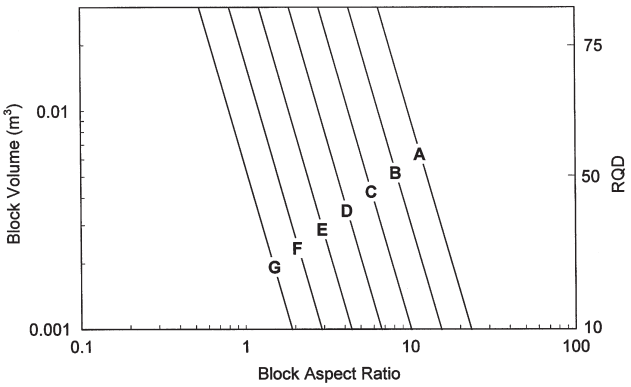

Figure 51—Classification of a rock mass on the basis of the aspect ratio parallel to the hangingwall skin and the volume of the blocks

SECTION 8

Support spacing requirements for blocky hangingwalls

The support spacing requirements described in the previous section are only applicable if the hangingwall stability is controlled by sliding and rotating of keyblocks, or by beam buckling. This section summarizes a second approach to support spacing requirements, which is particularly applicable for blocky hangingwall conditions (see Figure 49). The design charts are based on work conducted as part of SIMRAC project GAP335 (Haile *et al.*[36]), and can be used to design the spacing requirements of both prop and tendon support units. A fundamental assumption of the design procedure given here is that, when applied to tendon support, the tendons are anchored beyond the potentially unstable zone into the more competent overlying rock mass (i.e. beam suspension). Furthermore, if yielding tendons are used, the required yield length must lie above the potentially unstable zone (see Figure 50).

Haile *et al.*[36] found that the critical rock mass parameters determining the stability of blocky rock mass structures are the aspect ratio and the volume of the blocks. Based on the findings of numerical models, these two parameters were found to satisfactorily express the variations in size and geometry of the blocks that make up the rock mass structure, and reflect their relative stability. This correlation is best expressed in the form of a log-log plot, where linear divisions between the rock mass classes, which are based on the

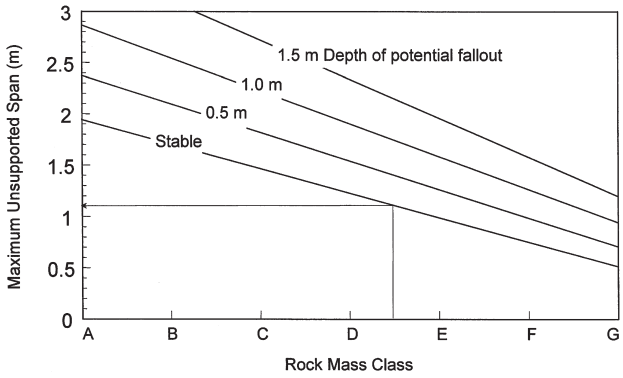

Figure 52—Maximum unsupported span for blocky rock mass structures as a function of rock mass class and depth of instability (rockfall conditions)

relative stability with regard to rock mass unravelling potential, are made (Figure 51). Also indicated on this chart are equivalent RQD (Rock Quality Designation) values as derived from the work of Palmstrøm[37].

Rockfall conditions

Once the rock mass classification is established, the stability of the rock mass between adjacent support units can be determined. This relationship, as derived from numerical modelling (Haile *et al.*[36]), is illustrated in Figure 52. The relationship is given as a function of depth of instability, from a completely stable span, to a 1.5 m depth of instability. In practice, the rock mechanics engineer should always design to achieve a stable span. In certain situations, however, a limited amount of rock fall-out between adjacent support units will be predicted to occur. If the resulting arches are unstable, areal coverage or reduced spacing of support units is required to prevent a rockfall hazard.

An example is given to illustrate the application of Figure 51 and Figure 52. Consider a blocky rock mass structure with blocks that are approximately 15 cm in length in the strike direction, 30 cm in the dip direction, with a thickness of 5 cm. This would give an average estimated block volume of 0.002 m³ and an average aspect ratio in the strike direction of 3 and in the dip direction of 6. For a simplified analysis the average aspect ratio (4.5) should be used. For a more detailed analysis the spacing in the strike and dip directions

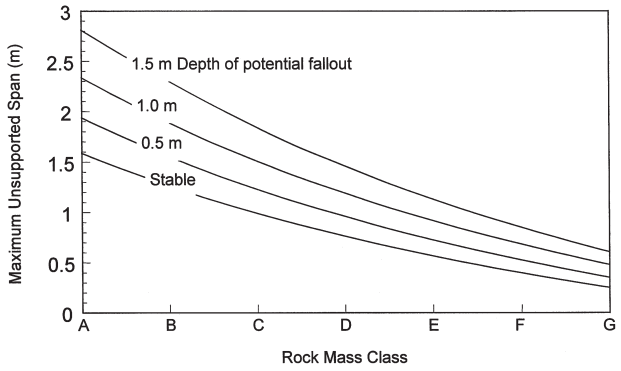

Figure 53—Maximum unsupported span for blocky rock mass structures as a function of rock mass class and depth of instability (rockburst conditions)

can be related to the aspect ratios in the corresponding directions, i.e. Figure 51and Figure 52 are used twice to determine the strike and dip spacing based on the respective aspect ratios.

From Figure 51, considering an aspect ratio of 4.5 and block volume of 0.002 m², a rock mass class of D/E is found. Using Figure 52, a rock mass class of D/E implies a maximum unsupported span of 1.1 m to ensure a stable hangingwall. The recommended support spacing is applicable for both prop and tendon support spacing, provided the tendons are long enough to be anchored in competent rock.

Rockburst conditions

For rockburst conditions Figure 51 is used to determine the appropriate rock mass class, based on the geometrical parameters of the blocks. Figure 53 is then applied to estimate maximum unsupported spans as a function of rock mass class and depth of instability. Figure 53 is based on dynamic correction factors established by Haile *et al.*[36], where the block ejection velocity is assumed to be 3 m/s and the reduced support spacing for dynamic conditions is proportional to the anticipated increase in the depth of instability.

SECTION 9

Choosing the appropriate support spacing based on tributary area calculations and maximum stable spans

Support spacing for hangingwalls with FPFs

The support design method gives insights into spacing and associated stable hangingwall spans in the strike direction only. Due to the face-parallel mining-induced fracture orientation in intermediate and deep level mines, the hangingwall rock is generally less prone to failure between two support units in the dip direction, compared to failure between units in the strike direction. Probabilistic keyblock analyses (Daehnke *et al.*[5]) have shown that, for a typical discontinuity spacing and attitude as encountered in intermediate depth and deep gold mines, the support spacing in the dip direction can be increased by a factor of ±1.5 compared with the strike spacing, while maintaining an equal probability of keyblock failure in the dip versus strike direction. Hence, to propose a prudent system, it is recommended that the support spacing in the dip direction can be up to but should not exceed 1.5 times the spacing in the strike direction. This simplifies the design procedure by eliminating the need for complicated three-dimensional analyses. Furthermore, this relationship has been found to be generally valid in practice, but, however, may not apply in blocky ground such as can be expected in sections of lagging panels which intersect siding parallel fractures.

In order to determine the strike and dip spacing of support units, the following calculation procedure is proposed.

The centre-to-centre strike spacing (s_S) of support units is calculated as:

$$S_s = \min\begin{cases}\sqrt{\dfrac{A_T}{1.5}} \\ S_{FPF} + w\end{cases}, \qquad [50]$$

where: A_T = maximum potential tributary area (from Figure 11 and Figure 14)
s_{FPF} = maximum stable span for hangingwalls with FPFs (from Figure 47 and Figure 48)
w = width of the support unit or headboard.

The unsupported span in the dip direction can be up to but must not exceed 1.5 times the unsupported span in the strike direction.

Support spacing for blocky hangingwalls

For blocky hangingwalls, the centre-to-centre strike spacing (s_S) of support units is calculated as:

$$S_s = \min\begin{cases}\sqrt{A_T} \\ S_B + w\end{cases}, \qquad [51]$$

where: A_T = maximum potential tributary area (from Figure 11 and Figure 14)
s_B = maximum stable span for blocky hangingwalls (from Figure 51, Figure 52 and Figure 53)
w = width of the support unit or headboard.

The centre-to-centre dip spacing of support units is recommended to be approximately equal to the centre-to-centre strike spacing.

SUPPORT DESIGN EXAMPLE

To illustrate the support design procedure, the optimum spacing of Loadmaster props in an intermediate depth mine for rockfall and rockburst conditions is determined. The height of instability (hangingwall beam thickness) is 1.0 m, the closure rate is 20 mm per metre of face advance, the stoping width is 1.6 m, and the hangingwall is discretized by extension and shear fractures dipping at 80° and 60°, respectively. The hangingwall is smooth, and the sliding, rotational and buckling failure of keyblocks governs the hangingwall stability.

Rockfall conditions

Determine force versus deformation characteristics of Loadmaster props:

By means of laboratory compression tests, the 1.6 m Loadmaster force versus deformation characteristics shown in Figure 54 were established (the characteristics of the most commonly used elongate types are given in Daehnke *et al.*[5]). laboratory compression tests were conducted and Figure 54 shows the mean of the ten tests, as well as the 90% probability curve (further details of

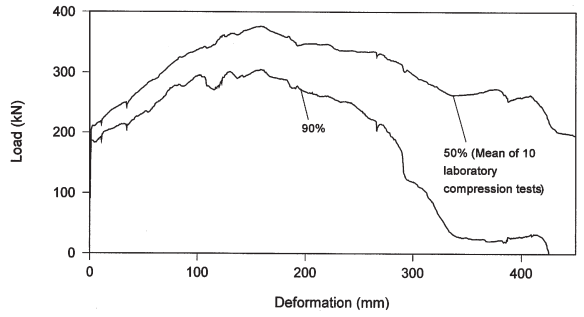

Figure 54—Force versus deformation characteristics of the Loadmaster prop

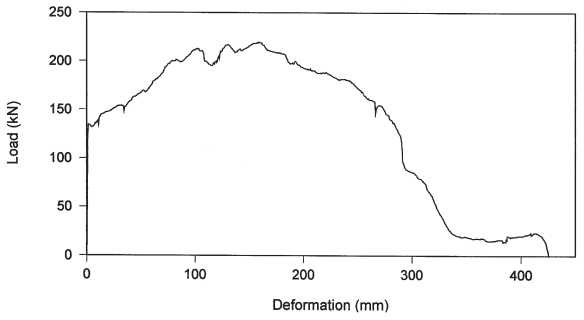

Figure 55—Corrected Loadmaster reference curve (90% probability)

probability curves are given by Daehnke[14]). In this example, the 90% probability curve is used as the reference force versus deformation curve of the Loadmaster prop.

The Loadmaster reference curve is downgraded for loading rate by the following Equation (Roberts[6]):

$$F_{u/g} = F_{lab}\left[m\log\left(\frac{v_{u/g}}{v_{lab}}\right)+1\right],$$

where: $F_{u/g}$ = adjusted force
F_{lab} = original force as measured during laboratory test
v_{lab} = laboratory test velocity
$v_{u/g}$ = underground site velocity
m = empirically determined correction factors,
where: m = 0.123 for rockbursts, and
m = 0.084 for rockfalls.

The corrected 90% design curve is shown in Figure 55 (v_{lab} = 30 mm/min, $v_{u/g}$ = 20 mm/day assuming the face is advanced every day).

Correction factors for stoping width are given by Roberts[6]. Since the stoping width in this example is 1.6 m, and the length of the laboratory tested Loadmaster was 1.6 m, no correction for prop height is necessary.

Tributary area spacing requirements

From Figure 55 it is apparent that the prop is initially set at a load of 135 kN. The yield load exceeds this value

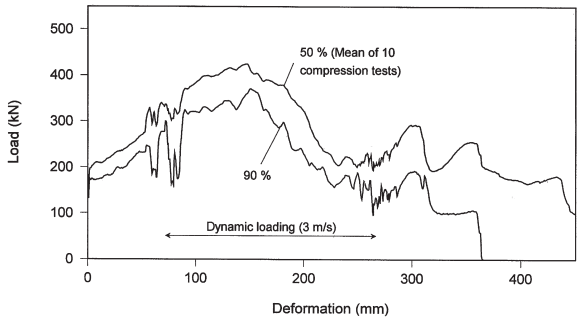

Figure 56—Dynamic force versus deformation characteristics of the Loadmaster prop

up to a total deformation of 285 mm. At a closure rate of 20 mm/m face advance, this implies that the prop will exceed 135 kN up to a distance of 14.25 m behind the stope face. This is considered a suitable working lifespan for the prop to ensure hangingwall stability in the working area, and hence the tributary area spacing requirements are based on a single support unit carrying 135 kN. From Figure 11 it is evident that, with F = 135 kN and height of instability b = 1.0 m, the maximum tributary area should not exceed 4.5 m².

Hangingwall with FPFs stability analysis

For extension and shear fracture angles of α = 80° and β = 60°, respectively, the light grey zone of Figure 47 is applicable (assuming a friction angle ϕ = 50°). The maximum unsupported span in the strike direction, at b = 1.0 m, is s_{FPF} = 2.2 m.

The recommended support spacing should be based on the minimum of the tributary area spacing and the maximum unsupported strike span requirements. When using props without headboards, the strike spacing (centre to centre) of the props is approximately equal to the unsupported span. Hence, $A_T = s_s \times s_d$, where A_T is the tributary area and s_s, s_d are the strike and dip spacing of support units. In this example $A_T \leq$ 4.5 m². Using Equation [50], the recommended centre-to-centre strike spacing (s_s) is calculated as:

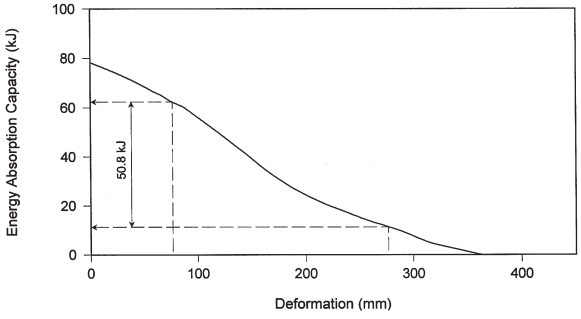

Figure 57—Energy absorption capacity of the Loadmaster prop

$$s_s = \min\begin{cases}\sqrt{\frac{A_T}{1.5}} \\ s_{FPF} + w\end{cases} = \min\begin{cases}\sqrt{\frac{4.5}{1.5}} = 1.73 \text{ m.} \\ 2.2\end{cases}$$

The dip spacing can be up to, but must not exceed, 1.5 s_S = 2.60 m. Thus, a strike spacing of 1.73 m and dip spacing of 2.60 m is recommended.

Rockburst conditions

Determine the energy absorption capacity of Loadmaster props

Figure 56 shows the force versus deformation characteristics of a Loadmaster prop loaded dynamically. The mean of ten laboratory compression tests, as well as the 90% probability curve, is given. The prop was initially compressed at a slow rate over a distance of 80 mm. Thereafter the prop was rapidly compressed at a rate of 3 m/s over a distance of 200 mm, followed once again by slow loading.

Figure 57 gives the remaining energy absorption capacity of the Loadmaster prop (based on the 90% reference curve given in Figure 56). From the graph it is apparent that between 80 mm and 280 mm dynamic compression, 50.8 kJ of energy is absorbed.

Tributary area spacing requirements

Assuming the prop is subjected to rockburst loading (3 m/s over 0.2 m) after 80 mm of quasi-static convergence, 50.8 kJ of energy can be absorbed. From Figure 14, at a height of instability of 1.0 m and 50 kJ, the maximum tributary area for rockburst conditions is found to be 2.9 m^2.

Further rockburst support criteria that need to be satisfied are:

(i) The load carried by the support unit after the rockburst must exceed the corresponding tributary area load. In this example F(280 mm) = 140 kN (from Figure 54), which is adequate to support the tributary area load = $\rho\ g\ b\ A_T$ = 78 kN.

(ii) The stoping width minus the total closure after the rockburst should be adequate to prevent injury to and allow movement of mine personnel (>0.6 m is recommended). In the example given here the initial stoping width is 1.6 m and thus the post-rockburst stoping width (1.6 m – 0.08 m – 0.2 m = 1.32 m) is adequate.

Note that by checking the energy absorption capacity of the prop after 80 mm of quasi-static convergence, it is implied that the prop will meet the rockburst criteria as the face is advanced a further 4 m (80 mm ÷ 20 mm/m face advance). At prop-to-face distances exceeding 4 m plus the installation distance from the face, the rockburst criteria are not necessarily met and the energy absorption capacity, post-rockburst support resistance or post-rockburst stoping width may be inadequate.

Hangingwall with FPFs stability analysis

For extension and shear fracture angles of α = 80° and β = 60°, respectively, the light grey zone of Figure 48 is applicable (assuming a friction angle of ϕ = 50°). The maximum unsupported span in the strike direction, at b = 1.0 m, is s_{FPF} = 1.9 m.

The centre-to-centre strike spacing (s_S) is calculated using Equation [50], i.e.

$$s_s = \min\begin{cases}\sqrt{\frac{A_T}{1.5}} \\ s_{FPF} + w\end{cases} = \min\begin{cases}\sqrt{\frac{2.9}{1.5}} = 1.39 \text{ m.} \\ 1.9\end{cases}$$

The dip spacing can be up to, but must not exceed, 1.5 s_S = 2.09 m. Thus, a maximum strike spacing of 1.39 m and dip spacing of 2.09 m is recommended.

Note that in the case of shallow dipping fractures (α < 40° and β < 40° if the fracture surface friction angle ϕ = 50°), the maximum strike spacing is limited to 0.75 m and 0.65 m for rockfall and rockburst conditions, respectively (determined from Figure 47 and Figure 48 for b = 1.0 m). In this case considerably closer support spacing and/or the use of strike parallel headboards is recommended.

Conclusions

Support design methodologies must be based on sound engineering principles to optimize support systems in terms of safety and cost. In this section some of the fundamental rock mass and support engineering criteria, that form the basis of an improved support design methodology, have been reviewed. The considered design criteria are (i) height of potential fall, (ii) quasi-static stope closure rates, (iii) dynamic stope closure rates, (iv) compressive hangingwall stresses, (v) discontinuity spacing, orientation and interface properties, (vi) effect of support length (stoping width), (vii) effect of compression rate, (viii) consistency of support performance, (ix) areal coverage, (x) support spacing, and (xi) zone of support influence.

The development of an improved support design methodology for rockfall and rockburst conditions has led to the potential for significant increases in worker safety and support cost savings. The site-specific methodology consists of two stages: (i) a tributary area analysis, and (ii) a zone of support influence and a stability analysis, considering hangingwall failure due to buckling, shear and block rotation, which gives maximum safe spacing of individual support units.

For hangingwall conditions in which both the stability of keyblocks, as well as the unravelling of a blocky rock mass structure governs the rock mass integrity, it is recommended to determine the maximum stable spans for both blocky hangingwalls and hangingwalls with face parallel fractures. In this case, the ultimate support spacing to be used should be the minimum of the blocky hangingwall and hangingwall with face parallel fractures analyses.

It is envisaged that, following *in situ* evaluation of support designed by the methodology given here, the method will be incorporated in a design program such as SDA II for use in the industry.

Further research needs to be conducted to quantify the effects of arbitrarily oriented discontinuities of geological origin on support spacing in the strike and particularly the dip directions. The horizontal clamping stress is a vital part of the design procedure. Further work needs to be done to clarify the magnitude and role of this important component, particularly during the passage of a train of seismic waves when clamping forces can be relaxed and increased.

Finally, the rock engineer should at all times apply his/her engineering judgement to design support systems offering a high probability of rock mass stability. The work presented here considers only two fundamental failure mechanisms and may well be unsuitable for particular geotechnical areas. At all times a conservative approach should be taken to support system design. For particularly complex rock mass structures and/or poorly understood failure mechanisms, support spacing should be further reduced and support resistance and energy absorption capacities increased.

Acknowledgements

The authors would like to thank the Safety in Mines Research Advisory Committee (SIMRAC) for their financial support. The authors are further indebted to A.J. Jager, Dr J.A. Ryder, D. Adams, Dr M. Handley and Dr T.O. Hagan for their guidance and valuable technical contribution.

References

1. Pretorius, P.G.D. Strata control and rockburst problems on central Witwatersrand gold mines, *Association of Mine Managers of South Africa.* 1973.
2. Klokow, J. Evaluation of current recommended stope support design methodology as applied to deep level mining. *Proc. of the Colloquium for Successful Support Systems for Safe and Efficient Mining,* 27 May 1999, South African Inst. of Mining and Metallurgy. 1999.
3. Daehnke, A., Andersen, L.M., Kuijpers, J.S. and Ntuli, J. Quantitative rock engineering criteria for effective stope support. Final Project Report, Deepmine Task 4.1.2. CSIR: Division of Mining Technology. 1999a. pp. 1–89.
4. Roberts, M.K.C. The Design of Stope Support Systems in South African Gold and Platinum Mines. Ph.D. thesis, University of Witwatersrand, Johannesburg. 1999.
5. Daehnke, A., Andersen, L.M., de Beer, D., Esterhuizen, G.S., Glisson, F.J., Grodner, M.W., Hagan, T.O., Jaku, E.P., Kuijpers, J.S., Peake, A.V., Piper, P.S., Quaye, G.B., Reddy, N., Roberts, M.K.C., Schweitzer, J.K., Stewart, R.D. and Wallmach, T. Stope face support systems. Final Report for SIMRAC Project GAP 330, CSIR: Division of Mining Technology. 1998. pp. 1–407.
6. Roberts, M.K.C. Stope and gully support. Final Report for SIMRAC Project GAP 032, CSIR: Division of Mining Technology. 1995. pp. 1–45.
7. Daehnke, A. Stress Wave and Fracture Propagation in Rock. Ph.D. Thesis, Vienna University of Technology. 1997.
8. Kirsten, H.A.D., and Stacey, T.R. Hangingwall behaviour in tabular stopes subjected to seismic events. *J.S. Afr. Inst. Min. Metall.*, 88(5). 1988. pp. 163–172.
9. Wagner, H. Support requirements for rockburst conditions. *Proc. of the 1st Int. Cong. on Rockbursts and Seismicity in Mines*, SAIMM, eds. N.C. Gay and E.H. Wainwright, Johannesburg, 1984. pp. 209–218.
10. CSIR: Division of Mining Technology. Reference report, No. 98-0332, Rock Engineering, Carlow Road, Auckland Park, 2006, Johannesburg, South Africa. 1998.
11. Jager, A.J. Personal communication, CSIR Mining Technology, Dec. 1999.
12. Jager, A.J. and Roberts, M.K.C. Support systems in productive excavations. *Gold 100. Proc. of the Int. Conf. on Gold*. Vol 1: Gold Mining Technology. SAIMM, Johannesburg, 1986. pp. 289–300.
13. COMRO 1988. An Industry Guide to Methods of Ameliorating the Hazards of Rockfalls and Rockbursts. *Chamber of Mines Research Organisation,* Johannesburg. 1988.
14. Daehnke, A. Addressing the reliability of elongate performance. *Jnl. S. A. Inst. Min. Metall.* vol. 101, 2001. pp. 83–90.
15. Shigley, J.E. *Mechanical Engineering Design.* McGraw-Hill Book Company. 1986.
16. Daehnke, A., Watson, B.P., Roberts, D., Acheampong, E. and Van Zyl, M. The impact of soft loading conditions on the performance of elongate support elements. Final Report for SIMRAC Project GAP 613, CSIR: Division of Mining Technology. 2000.
17. Roberts, M.K.C., Jager, A.J. and Riemann, K. The performance characteristics of timber props. Chamber of Mines Report no. 35/87. 1987.
18. Lightfoot, N. Support adjustment specification. Internal report RE97. CSIR: Division of Mining Technology. Auckland Park, South Africa. 1997.
19. Pretorius, M.J. A mathematical model to quantify stope support reaction. *Proceedings of the 2nd Southern African Rock Engineering Symposium,* Johannesburg, 13-15 September. 1999. pp. 204–215.
20. Jager, A.J. and Ryder, J.A. A Handbook on Rock Engineering Practice for Tabular Hardrock Mines. Johannesburg, *Department of Mineral and Energy Affairs.* 1999.
21. Kuijpers, J.S. Personal communication, CSIR Mining Technology, November 1999.
22. Daehnke, A., Salamon, M.D.G. and Roberts, M.K.C. Investigating zones of support influence and quantifying stable hangingwall spans between support units. To be published in: *J. of South African Inst. of Mining and Metall.* 1999b.
23. Evans, W.H. The strength of undermined strata. *Trans Instn Min. Metall.,* 50, 1941. pp. 475–532.
24. Beer, G. and Meek, J.L. Design curves for roofs and hangingwalls in bedded rock based on voussoir beam and plate solutions. *Trans Instn Min. Metall.,* 91, 1982. pp. A18–22.
25. Brady, B.H.G. and Brown, E.T. *Rock Mechanics For Underground Mining*. London: George Allen and Unwin. 1985.
26. Hutchinson, D.J. and Diederichs, M.S. *Cablebolting in Underground Mines.* BiTech Publishers, 1996. pp. 265–269.
27. Bandis, S.C., Lumsden, A.C. and Barton, N.R. Experimental studies of scale effects on the shear behaviour of rock joints. *International Journal of Rock Mech. Min. Sci. & Geomech.* Abstr., 1981. pp. 1 – 21.
28. Bandis, S.C., Lumsden, A.C. and Barton, N.R. Fundamentals of rock joint deformation. *International Journal of Rock Mech. Min. Sci. & Geomech.* Abstr., 20(6), 1983. pp. 249–268.
29. Esterhuizen, G.S. Analysis of keyblock rotation in Bushveld mines. Interim report for SIMRAC Project GAP 613, Elongate support performance and requirements of blocky rock masses. 1999.
30. Daehnke, A., Le Bron, K. and Van Zyl, M. Preliminary Investigation into the Zone of Support Influence and Stable Span between Support Units. Final Report for SIMRAC Project GAP 627, CSIR: Division of Mining Technology, 1999c. pp. 1–151.
31. ITASCA. Universal Distinct Element Code (UDEC), Version 2 Manual. 1993.
32. CSIR: Division of Mining Technology. Support Design Analysis (SDA II) software. Rock Engineering, Carlow Road, Auckland Park 2006, Johannesburg, South Africa. 1999.
33. Squelch, A.P. The Determination of the Influence of Backfill on Rockfalls in South African Gold Mines. M.Sc. dissertation, University of Witwatersrand, Johannesburg. 1994.
34. Herrmann, D.A. Fracture Control in the Hangingwall and the Interaction Between the Support System and the Overlying Strata. M.Sc. dissertation, University of the Witwatersrand, Johannesburg. 1987.
35. Ryder, J.A. Personal communication, CSIR Mining Technology, Dec. 1999.
36. Haile, A.T., Grave, D.M., Sevume, C. and Le Bron, K. Strata control in tunnels and an evaluation of support units and systems currently used with a view to improving the effectiveness of support, stability and safety of tunnels. SIMRAC GAP335 Project Report. CSIR: Division of Mining Technology. 1998.
37. Palmstrøm, A. Characterising rock masses by the RMi for use in practical rock engineering Part 1: The development of the Rock Mass Index (RMi), *Tunnelling and Underground Space Technology,* volume 11, no.2. Pergamon Press. 1996. ◆